

Shell-confined atom and plasma: incidental degeneracy, metallic character and information entropy

Neetik Mukherjee* and Amlan K. Roy†

Department of Chemical Sciences

Indian Institute of Science Education and Research (IISER) Kolkata,

Mohanpur-741246, Nadia, WB, India

Abstract

Shell confined atom can serve as a generalized model to explain both *free* and *confined* condition. In this scenario, an atom is trapped inside two concentric spheres of inner (R_a) and outer (R_b) radius. The choice of R_a, R_b renders four different quantum mechanical systems. In hydrogenic atom, they are termed as (a) free hydrogen atom (FHA) (b) confined hydrogen atom (CHA) (c) shell-confined hydrogen atom (SCHA) (d) left-confined hydrogen atom (LCHA). By placing R_a, R_b at the location of radial nodes of respective *free* n, ℓ states, a new kind of degeneracy may arise. At a given n of FHA, there exists $\frac{n(n+1)(n+2)}{6}$ number of iso-energetic states with energy $-\frac{Z^2}{2n^2}$. Furthermore, within a given n , the individual contribution of each of these four potentials has also been enumerated. This incidental degeneracy concept is further explored and analyzed in certain well-known *plasma* (Debye and exponential cosine screened) systems. Multipole oscillator strength, $f^{(k)}$, and polarizability, $\alpha^{(k)}$, are evaluated for (a)-(d) in some low-lying states ($k = 1 - 4$). In excited states, *negative* polarizability is also observed. In this context, metallic behavior of H-like systems in SCHA is discussed and demonstrated. Additionally analytical closed-form expression of $f^{(k)}$ and $\alpha^{(k)}$ are reported for $1s, 2s, 2p, 3d, 4f, 5g$ states of FHA. Finally, Shannon entropy and Onicescu **information** energies are investigated in ground state in SCHA and LCHA in both position and momentum spaces. Much of the results are reported here for first time.

PACS: 03.65.-w, 03.65.Ca, 03.65.Ge, 03.67.-a.

Keywords: Shell confinement, incidental degeneracy, polarizability, oscillator strength, metallic character, Shannon entropy, Onicescu **information** energy.

*Email: pchem.neetik@gmail.com.

†Corresponding author. Email: akroy@iiserkol.ac.in, akroy6k@gmail.com.

I. INTRODUCTION

The discovery and development of modern scientific techniques has triggered an invasive interest on confined quantum systems. Particularly, in such environment, the rearrangement of atomic orbitals and increase in coordination number may lead to some fascinating, exceptional changes in physical and chemical characteristics [1], such as, room temperature superconductivity [2], metallic behavior in ground state of H-like atoms [3] etc. These confined systems have profound applications in condensed matter physics, high energy physics, astrophysics and nanotechnology [4, 5]. The idea of quantum confinement has been exploited in construction of *artificial atom* or a *quantum dot* [6]. Such systems typically consist of a group of electrons confined within a potential well. Another important example is the encapsulation of an atom or molecule in fullerene cage or zeolite cavity [7–9].

Atomic polarization plays a key role in explaining a number of processes in physics and chemistry. For example, multipole polarizability of an atom reflects quantitative distortion in electronic charge distribution due to presence of an external electromagnetic field. A host of macroscopic properties like refractive index, dielectric constant can be estimated via dipole polarizability [10]. The latter plays an important role in the determination of physico-chemical properties, like optical response, as well as atomic and molecular interactions [11].

Originally, the confinement model was proposed to understand changes in static dipole polarizability of H atom due to the influence of effective pressure acting on a given surface [12]. In this fundamental system, H atom was trapped inside an impenetrable spherical cavity. The results of the designed model was utilized to gain knowledge of the core of planets like jupiter and saturn [13, 14]. Of late, this concept was extended to a number of other physical, chemical and biological systems. A considerable amount of theoretical work has been published, covering a large variety of confining potentials [1, 4] resulting in a vast literature. A confined H atom (CHA) in a spherical enclosure [15–22] represents a prototypical system, whose Schrödinger equation (SE) can be solved *exactly* [17, 23] in terms of *Kummer confluent Hypergeometric* function. Hydrogen atom under the influence of several *penetrable* as well as *impenetrable* cavity was explored with great enthusiasm, giving rise to several interesting attractive properties—both from chemical and physical point of view. They offer some unique phenomena, especially the rearrangement of atomic orbitals, *simultaneous*, *incidental* and *inter-dimensional* degeneracy [23] etc. Recently a new virial-like

theorem is also formulated for such confinement situation [24]. Moreover, various properties like hyper-fine splitting constant, dipole shielding factor, nuclear magnetic screening constant, static, and dynamic polarizability, information entropy, Compton profiles [25–31] were examined for CHA. Further, the information theoretic measures are investigated for H-like atoms in Debye plasmas [32]. A recent study reports the influence of external electric field on total Shannon entropy (S_t) [33]. Benchmark results for Rényi, Tsallis entropies and Onicescu information energy (E^O) for ground state of Helium atom was studied using Hylleraas method [34]. The static multipole polarizabilities are estimated for H-like atoms in Hulthén potential under both *confined* and *free* conditions [35] and H-atom in ring-shaped potentials [36]. Moreover, generalized pseudospectral (GPS) method was used to explore several spectroscopic properties like fine structure, hyperfine splitting in confined environment [37]. Photoionization in H-atoms under fullerene cage is also reported for low-lying *s*-states [38]. However, an in-depth analysis of multipole oscillator strength and polarizability are yet to be done for H atom trapped inside a cage, which remains one of the objectives of this work.

A shell confinement model provides a new, unique boundary condition [3, 39, 40]. An appropriate choice of inner (R_a) and outer (R_b) radius of the shell can describe all possible radial boundary conditions so far reported in literature. For instance, when $R_a = 0, R_b = r_c$ (r_c is a real finite number) it reduces to CHA. On the other hand, choosing $R_a = 0, R_b = \infty$, a *free* H atom (FHA) is achieved. When both R_a, R_b are non-zero and finite, it is termed as *shell confined H-like atom* (SCHA). Whereas, a *finite* R_a and *infinite* R_b indicates *left confined H-like atom* (LCHA). All these four systems, in general, are referred as a *generalized confined H atom* (GCHA). The nodal characteristics of orbitals of FHA have played a significant role in conceptual development of degeneracy in GCHA. Previously, an attempt was made to solve SE of SCHA *exactly* [40], with limited success. Later, an accurate numerical strategy [3, 41] was prescribed to emphasize the occurrence of incidental degeneracy in SCHA [39]. This new degeneracy can also account for the presence of incidental and simultaneous degeneracy in a CHA. The Kirkwood [42] and Buckingham [43] polarizability were evaluated [39]. Sternheimer perturbation-numerical method [44] was employed to calculate dipole polarizability in ground state [39]. The Buckingham results are in good agreement with polarizability obtained via perturbation numerical procedure [3]. The higher value of dipole polarizability in SCHA indicates metallic behavior of H atom in ground state [3]. Eigenvalues and eigenfunctions of D -dimensional SCHA has been examined lately [45].

In practice, a prototypical example of shell confinement is encapsulation of an atom or molecule under fullerene cage and zeolite cavity [46] or inside *metal organic framework* [47, 48]. Such an environment enhances stability and activity of *noble-metal* catalysts by inhibiting the sintering effect [48–52], amplifies photoluminescence in nano crystals by reducing non-radiative Auger processes [47, 53] and removes defects in polymer crystals [54, 55] etc. Apart from these examples, shell confinement has potential applications in pollution control [56, 57], therapeutics [58] and energy storage [59–61].

In spite of having such versatile characteristics, shell confinement model has been studied only sparingly. As a consequence, literature on the topic is rather scarce. In this endeavour, our primary objective is to explore SCHA systematically, mainly through energy and other characteristic properties. Towards this goal, we consider incidental degeneracy, multipole (2^k -pole) oscillator strength, $f^{(k)}$ and polarizability, $\alpha^{(k)}$ ($k = 1 - 4$), as well as certain information measures like S and E^O in ground and a few low-lying states. Here $k = 1 - 4$ represent dipole, quadrupole, octupole and hexadecapole moments successively. In GCHA model, dependence of this degeneracy on principal (n) and orbital (ℓ) quantum numbers is analyzed. This helps us to find out the exact number of degenerate states (in GCHA) associated with a given FHA energy of the form $-\frac{Z^2}{2n^2}$. Further, we can also estimate the number of such degenerate states that exists in GCHA. The calculation of dipole polarizability will guide us to examine the existence of metallic character in excited states. To this end, pilot calculations are performed on ground and lower excited states by invoking GPS method. To the best of our knowledge, most of the outcomes are presented here for first time. The article is constructed in following parts: Sec. II provides a brief description about the formalism employed in present work. Section III offers a detailed discussion of results. Finally, we conclude with a few remarks in Sec. IV.

II. THEORETICAL FORMALISM

The single-particle time-independent non-relativistic radial SE for a spherically confined system is expressed (atomic unit employed unless otherwise stated) as,

$$\left[-\frac{1}{2} \frac{d^2}{dr^2} + \frac{\ell(\ell+1)}{2r^2} + V_c(r) \right] \psi_{n,\ell}(r) = \mathcal{E}_{n,\ell} \psi_{n,\ell}(r), \quad (1)$$

where V_c represents the desired confined potential given below [3, 39],

$$V_c(r) = \begin{cases} = v(r) & \text{for } R_a \leq r \leq R_b \\ = \infty & \text{for } 0 \leq r \leq R_a \\ = \infty & \text{for } r \geq R_b. \end{cases} \quad (2)$$

Here, $v(r) = -\frac{Z}{r}$, signifies the electron-nuclear Coulomb attraction potential (Z refers to nuclear charge). Throughout our work, $V_c(r)$ will be referred as GCHA. Depending upon the values of R_a, R_b , four distinct possibilities can be envisaged, as in the following,

1. When $R_a = 0, R_b = \infty$, it gives rise to FHA.
2. When $R_a = 0, R_b = r_c$, a finite number, it corresponds to CHA.
3. When $R_a \neq 0, R_b \neq \infty$, with R_a, R_b finite, it signifies SCHA.
4. If $R_a \neq 0, R_b = \infty$, it refers to LCHA.

In order to calculate the energy, spectroscopic properties and information entropy the GPS method was invoked. **This provides a *non-uniform, optimal* spatial discretization maintaining, high accuracy at both small and large distances. In contrast to the standard finite-difference methods, reasonably smaller number of grid point suffices, as it facilitates a denser mesh at small r , while a coarser mesh at large r . Further, by applying a *symmetrization* technique and a *non-linear* mapping procedure, a *symmetric* eigenvalue equation is achieved. It is computationally orders of magnitude faster than finite-difference or finite element methods. Thus in essence, it combines the simplicity of direct finite-difference or finite element method, with the fast convergence of finite basis set approaches. Over the time, it has been successfully used to estimate various bound-state properties of several central potentials including energy and other properties in CHA and confined many-electron atom [24, 25, 29, 62–66],**

A. Multipole polarizability

By definition, the static multipole polarizability can be conveniently written as,

$$\alpha_i^{(k)} = \alpha_i^{(k)}(\text{bound}) + \alpha_i^{(k)}(\text{continuum}). \quad (3)$$

Conventionally $\alpha_i^{(k)}$ is expressed in terms of compact sum-over states form [67]. However it can also be directly estimated by employing the standard perturbation theory framework [68]. In the first procedure, Eq. (4) modifies to [69],

$$\begin{aligned}\alpha_i^{(k)} &= \sum_n \frac{f_{ni}^{(k)}}{(\mathcal{E}_n - \mathcal{E}_i)^2} - c \int \frac{|\langle R_i | r^k Y_{kq}(\mathbf{r}) | R_{\epsilon p} \rangle|^2}{(\mathcal{E}_{\epsilon p} - \mathcal{E}_i)} d\epsilon, \\ \alpha_i^{(k)}(\text{bound}) &= \sum_n \frac{f_{ni}^{(k)}}{(\Delta\mathcal{E}_{ni})^2}, \quad \alpha_i^k(\text{continuum}) = c \int \frac{|\langle R_i | r^k Y_{kq}(\mathbf{r}) | R_{\epsilon p} \rangle|^2}{(\mathcal{E}_{\epsilon p} - \mathcal{E}_i)} d\epsilon.\end{aligned}\tag{4}$$

In Eq. (4), the summation and integral terms signify bound and continuum contributions respectively, $f_{ni}^{(k)}$ represents multipole oscillator strength (k is a positive integer), c is a *real* constant depending only on ℓ quantum number. **q is an integer.** Here, $f_{ni}^{(k)}$ measures the mean probability of transition between an initial (i) to final (n) state, which is normally expressed as,

$$f_{ni}^{(k)} = \frac{8\pi}{(2k+1)} \Delta\mathcal{E}_{ni} |\langle r^k Y_{kq}(\mathbf{r}) \rangle|^2.\tag{5}$$

Designating the initial and final states as $|n\ell m\rangle$ and $|n'\ell' m'\rangle$, one can easily derive,

$$f_{ni}^{(k)} = \frac{8\pi}{(2k+1)} \Delta\mathcal{E}_{ni} \frac{1}{2\ell+1} \sum_m \sum_{m'} |\langle n'\ell' m' | r^k Y_{kq}(\mathbf{r}) | n\ell m \rangle|^2.\tag{6}$$

The application of Wigner-Eckart theorem and sum rule for $3j$ symbol further leads to,

$$f_{ni}^{(k)} = 2 \frac{(2\ell'+1)}{(2k+1)} \Delta\mathcal{E}_{ni} |\langle r^k \rangle_{n\ell}^{n'\ell'}|^2 \left\{ \begin{matrix} \ell' & k & \ell \\ 0 & 0 & 0 \end{matrix} \right\}^2.\tag{7}$$

The transition matrix element is then given by following radial integral,

$$\langle r^k \rangle = \int_0^\infty R_{n'\ell'}(r) r^k R_{n\ell}(r) r^2 dr.\tag{8}$$

Note that, $f_{ni}^{(k)}$ depends on n, ℓ , but independent of magnetic quantum number m . In this article, we compute $f^{(k)}$, $\alpha^{(k)}$, having $k = 1 - 4$, for states with $\ell = 0 - 4$. It is necessary to point out that, there exists a multipole oscillator strength sum rule as follows,

$$S^{(k)} = \sum_m f^{(k)} = k \langle \psi_i | r^{(2k-2)} | \psi_i \rangle,\tag{9}$$

where the summation includes all the bound and continuum states.

B. Information entropy

Information entropic measures are functionals of density and they quantify density in several complimentary ways. They have potential applications in atomic avoided crossing, electron correlation effect, quantum entanglement, orbital-free density functional theory etc [25, 29]. S is the arithmetic mean of uncertainty, and expressed as an expectation value of logarithmic density. $S_{\mathbf{r}}$ measures the uncertainty in localization of a particle in r space. A lower $S_{\mathbf{r}}$ indicates higher accuracy in predicting the localization. Similarly, $S_{\mathbf{p}}$ measures the uncertainty in predicting the momentum of a particle. $S_{\mathbf{r}}$ and $S_{\mathbf{p}}$ are expressed as,

$$\begin{aligned} S_{\mathbf{r}} &= - \int_{\mathcal{R}^3} \rho(\mathbf{r}) \ln[\rho(\mathbf{r})] d\mathbf{r} = 2\pi (S_r + S_{(\theta,\phi)}), \\ S_{\mathbf{p}} &= - \int_{\mathcal{R}^3} \Pi(\mathbf{p}) \ln[\Pi(\mathbf{p})] d\mathbf{p} = 2\pi (S_p + S_{(\theta,\phi)}). \end{aligned} \quad (10)$$

Here $\rho(\mathbf{r})$, $\Pi(\mathbf{p})$ signify r - and p -space densities, both normalized to unity. Arguably, $S_{\mathbf{r}}$ and $S_{\mathbf{p}}$ provide the most appropriate uncertainty relation [70]. $S_{\mathbf{r}}$ and $S_{\mathbf{p}}$ are the logarithmic functionals of density. As a consequence, the total Shannon entropy is expressed as $S_{\mathbf{r}} + S_{\mathbf{p}}$,

$$S_t = S_{\mathbf{r}} + S_{\mathbf{p}} = 2\pi [S_r + S_p + 2S_{(\theta,\phi)}] \geq 3(1 + \ln \pi). \quad (11)$$

The quantities S_r , S_p and S_{θ} are defined as [70],

$$\begin{aligned} S_r &= - \int_0^{\infty} \rho(r) \ln[\rho(r)] r^2 dr, & S_p &= - \int_0^{\infty} \Pi(p) \ln[\Pi(p)] p^2 dp, \\ \rho(r) &= |\psi_{n,l}(r)|^2, & \Pi(p) &= |\psi_{n,l}(p)|^2, \\ S_{(\theta,\phi)} &= - \int_0^{\pi} \chi(\theta) \ln[\chi(\theta)] \sin \theta d\theta, & \chi(\theta) &= |\Theta(\theta)|^2. \end{aligned} \quad (12)$$

Another important measure studied in this work is E^O , referring to the 2nd order entropic moment [31]. It is the expectation value of density. It portrays exactly opposite behavior to S . It is also termed as dis-equilibrium, as it measures the deviation of a distribution from equilibrium [71]. In r and p space, the respective quantities are defined as,

$$E_r^O = \int_0^{\infty} [\rho(r)]^2 r^2 dr, \quad E_p^O = \int_0^{\infty} [\Pi(p)]^2 p^2 dp, \quad E_{\theta,\phi}^O = \int_0^{\pi} [\chi(\theta)]^2 \sin \theta d\theta, \quad E_t^O = E_r^O E_p^O [E_{\theta,\phi}^O]^2. \quad (13)$$

where, E_t^O is the total Onicescu information energy. Accurate r -space wave functions are obtained by applying GPS method. The corresponding p -space wave function is generated by Fourier transforming the r -space counterpart. This is accomplished quite efficiently by following a procedure adopted in [25].

III. RESULT AND DISCUSSION

In [39], all three (CHA, SCHA, LCHA) models were mentioned under the general SCHA heading. However, since they have quite different energy characteristics, we discuss them separately here. The demonstrative results are presented for H-atom ($Z = 1$) only. However, similar outcome can also be extracted for $Z \neq 1$ cases. Thus, at first, we shall analyze the salient features of incidental degeneracy achieved by placing the boundary at respective nodal positions of FHA. Then we present $f^{(k)}(Z)$ and $\alpha^{(k)}(Z)$ ($k = 1 - 4$) for selected low-lying states in these four potentials. Further, in the realm of Herzfeld criterion of metallic behavior, we have computed $\alpha^{(1)}(Z)$ for $1s, 2s, 2p, 3d, 4f, 5g$ states. As a bonus, analytical closed-form expressions of $f^{(k)}(Z)$ and $\alpha^{(k)}(Z)$ are derived for all these six states. Finally, we consider S_r, S_p, S as well as E_r^O, E_p^O, E in ground state involving these four potentials. It is noteworthy to mention that, in case of degeneracy, radial boundaries are chosen specifically at the nodes of FHA to illustrate their role. Whereas for other properties ($f^{(k)}, \alpha^{(k)}$, information entropy), no such factor was taken into consideration. Thus they are selected so as to illustrate the essential features related to an individual property.

A. Incidental Degeneracy

Following [39], it may so happen that, the energy of a given confined state becomes equal to that of an unconfined state (here it is $-\frac{Z}{2n^2}$), when the radius of confinement is suitably chosen at the location of radial nodes in latter state. Such a phenomenon is termed as *incidental degeneracy*. It is shown in Eq. (2) that, *shell confined* condition renders four different systems. This degeneracy may provide a connection amongst them.

1. H-like ion

It is known that, if R_a, R_b of a GCHA coincide with certain specific radial nodes of (n, ℓ) state of FHA, then there exists $(n' - \ell - 1)$ number of nodes in between them. Furthermore, energy of such a (n', ℓ) GCHA state becomes degenerate to that of a FHA state. At first, we wish to determine the *number of degenerate states* associated with a given FHA energy $-\frac{Z^2}{2n^2}$. It is worthwhile mentioning that, in this part we shall only discuss the states that arises due to placing the boundary at nodal points of FHA. For demonstrative purpose, we present all

TABLE I: Incidental degeneracy in GCHA associated with $n = 4$ of FHA. See text for details.

Serial	No. of node	State	R_a	R_b	Energy	FHA	$\alpha^{(1)}$	S_r
<i>a</i>	0	1 <i>s</i>	0	1.87164450	-0.03125000	4 <i>s</i>	0.27404101	2.22927677
<i>b</i>	0	1 <i>s</i>	1.87164450	6.6108150	-0.03125000	4 <i>s</i>	169.7527968	6.55734580
<i>c</i>	0	1 <i>s</i>	6.6108150	15.51755	-0.03125000	4 <i>s</i>	8609.5280939	9.15073565
<i>d</i>	0	1 <i>s</i>	15.51755	100	-0.03125000	4 <i>s</i>	322925.0793	12.14484806
<i>e</i>	1	2 <i>s</i>	0	6.6108150	-0.03125000	4 <i>s</i>	-128.96450306	6.35223141
<i>f</i>	1	2 <i>s</i>	1.87164450	15.51755	-0.03125000	4 <i>s</i>	2265.40684074	9.10240049
<i>g</i>	1	2 <i>s</i>	6.6108150	100	-0.03125000	4 <i>s</i>	173868.83409	12.14272018
<i>h</i>	2	3 <i>s</i>	0	15.51755	-0.03125000	4 <i>s</i>	129.09470914	9.01151759
<i>i</i>	2	3 <i>s</i>	1.87164450	100	-0.03125000	4 <i>s</i>	80408.86663	12.09689745
<i>j</i>	3	4 <i>s</i>	0	100	-0.03125000	4 <i>s</i>	4992.00000000	12.07490387
<i>k</i>	0	2 <i>p</i>	0	10-2 $\sqrt{5}$	-0.03125000	4 <i>p</i>	13.56524044	5.42877070
<i>l</i>	0	2 <i>p</i>	10-2 $\sqrt{5}$	10+2 $\sqrt{5}$	-0.03125000	4 <i>p</i>	1711.37938497	8.51079967
<i>m</i>	0	2 <i>p</i>	10-2 $\sqrt{5}$	125	-0.03125000	4 <i>p</i>	84939.073612	11.63160747
<i>n</i>	1	3 <i>p</i>	0	10+2 $\sqrt{5}$	-0.03125000	4 <i>p</i>	-977.65896463	8.32046807
<i>o</i>	1	3 <i>p</i>	10-2 $\sqrt{5}$	105	-0.03125000	4 <i>p</i>	40632.47423	11.61219021
<i>p</i>	2	4 <i>p</i>	0	125	-0.03125000	4 <i>p</i>	5107.1999999	11.53386387
<i>q</i>	0	3 <i>d</i>	0	12	-0.03125000	4 <i>d</i>	203.03802379	7.82189131
<i>r</i>	0	3 <i>d</i>	12	120	-0.03125000	4 <i>d</i>	18.72296856	11.37785020
<i>s</i>	1	4 <i>d</i>	0	125	-0.03125000	4 <i>d</i>	5760.000000	11.26209911
<i>t</i>	2	4 <i>f</i>	0	130	-0.03125000	4 <i>f</i>	6720.000000	10.86085521

the 10 states belonging to $n \leq 4$ of GCHA in Table I. The corresponding boundaries are chosen from radial nodes of 4*s*, 4*p*, 4*d* states of FHA. Thus as can be seen, there exists a total of 20 degenerate states in GCHA, all having the same energy of -0.031250 a.u., corresponding to $n = 4$ of FHA. Out of that, the number of *s*, *p*, *d*, *f* are 10, 6, 3, 1 respectively. It is also recognized that, there are 6(*a*, *e*, *h*, *k*, *n*, *q*), 4(*b*, *c*, *f*, *l*), 6(*d*, *g*, *i*, *m*, *o*, *r*), 4(*j*, *p*, *s*, *t*) states belonging to CHA, SCHA, LCHA and FHA. The last two columns also tabulate the respective $\alpha^{(1)}$ ($\Delta\ell = 1$) and S_r . One can see that, in SCHA $\alpha^{(1)}$ possesses higher value compared to CHA and FHA counterparts.

It is well known that, in FHA, energies of all the ℓ states (0 to $n - 1$) within a given n are same. Now, from an observation of the results in Table I, it can be extracted that, there appears $\frac{(n-\ell)(n-\ell+1)}{2}$ number of iso-energetic states in GCHA. Thus, for a given n -state

TABLE II: Incidental degeneracy in WCP and ECSCP, for $\lambda_1, \lambda_2 = 0.01$ a.u. See text for details.

Serial	No. of node	State	R_a	R_b	Energy	Free state	$\alpha^{(1)}$	S_r
WCP								
2a	0	1s	0	2.000390	-0.115293282	2s	0.34278641	2.39716825
2b	0	1s	2.000390	100	-0.115293282	2s	932.14066065	8.21415856
2c	1	2s	0	100	-0.115293282	2s	120.5848668	8.11443243
3a	0	1s	0	1.902698	-0.046198857	3s	0.28975431	2.27113719
3b	0	1s	1.902698	7.108762	-0.046198857	3s	208.23885866	6.75134003
3c	0	1s	7.108762	150	-0.046198857	3s	28579.047941	10.53960365
3d	1	2s	0	7.108762	-0.046198857	3s	-207.14861496	6.56892996
3e	1	2s	1.9026980	150	-0.046198857	3s	12624.6506	10.48406780
3f	2	3s	0	150	-0.046198857	3s	1033.70055187	10.44196440
4a	0	1s	0	1.8729343	-0.022356120	4s	0.27468622	2.23104252
4b	0	1s	1.8729343	6.6268050	-0.022356120	4s	170.96931921	6.56397087
4c	0	1s	6.6258050	15.6046240	-0.022356120	4s	8757.380222	9.16720124
4d	0	1s	15.6046240	150	-0.022356120	4s	337593.5180	12.18838925
4e	1	2s	0	6.6268050	-0.022356120	4s	-131.07497378	6.35963966
4f	1	2s	1.8729343	15.6046240	-0.022356120	4s	2309.54693312	9.11891006
4g	1	2s	6.6268050	150.0	-0.022356120	4s	182824.8322	12.18544076
4h	2	3s	0	15.6046240	-0.022356120	4s	131.30125522	9.02899807
4i	2	3s	1.8729343	150	-0.022356120	4s	85268.9345	12.14058812
4j	3	4s	0	150	-0.022356120	4s	5294.641728	12.11924015
ECSCP								
2a	0	1s	0	2.0000208	-0.115013458	2s	0.34257005	2.39669558
2b	0	1s	2.0000208	100	-0.115013458	2s	928.75702501	8.21114396
2c	1	2s	0	100	-0.115013458	2s	120.07106878	8.11127833
3a	0	1s	0	1.90200530	-0.045619079	3s	0.28939390	2.27020331
3b	0	1s	1.90200530	7.0994429	-0.045619079	3s	207.43129440	6.74776731
3c	0	1s	7.0994429	150	-0.045619079	3s	28215.90613	10.52774639
3d	1	2s	0	7.0994429	-0.045619079	3s	-205.22594788	6.56497789
3e	1	2s	1.902000530	150	-0.045619079	3s	12430.91176	10.47209351
3f	2	3s	0	150	-0.045619079	3s	1017.71439735	10.42967937
4a	0	1s	0	1.87185526	-0.021437465	4s	0.27414583	2.22956395
4b	0	1s	1.87185526	6.61372660	-0.021437465	4s	169.96865645	6.55854163
4c	0	1s	6.61372660	15.5362170	-0.021437465	4s	8639.641193	9.15424609
4d	0	1s	15.5362170	150	-0.021437465	4s	327409.3061	12.15969133
4e	1	2s	0	6.61372660	-0.021437465	4s	-129.33805232	6.35357332
4f	1	2s	1.87185526	15.5362170	-0.021437465	4s	2274.9433235	9.10593888
4g	1	2s	6.61372660	150.0	-0.021437465	4s	176835.0570	12.15740646
4h	2	3s	0	15.6046240	-0.021437465	4s	129.58544973	9.02879432
4i	2	3s	1.87185526	150	-0.021437465	4s	82114.5084	12.11197447
4j	3	4s	0	150	-0.021437465	4s	5112.60426	12.09022342

of FHA, the total number of degenerate GCHA states work out to be,

$$\begin{aligned}
&= \frac{1}{2} \sum_{\ell=0}^{(n-1)} (n-\ell)(n-\ell+1) = \frac{1}{2} \sum_{\ell=0}^{(n-1)} (n-\ell)^2 + \sum_{\ell=0}^{n-1} (n-\ell) \\
&= \frac{n(n+1)}{2} + \frac{n(n+1)(2n+1)}{12} \\
&= \frac{n(n+1)(n+2)}{6}.
\end{aligned} \tag{14}$$

It suggests that, this number *does not* depend on ℓ . Now, we can determine the contribution of each of these four categories in this degeneracy, as follows.

(I) **FHA:** For a particular n , there exists n number of degenerate states.

(II) **CHA:** In this case, an ℓ -orbital contributes $(n-\ell-1)$ number of degenerate states.

Thus, the total number of degenerate states are then given by,

$$\sum_{\ell=0}^{(n-1)} (n-\ell-1) = \frac{n(n-1)}{2}. \tag{15}$$

(III) **SCHA:** In s orbital, first SCHA state occurs with energy equal to $n=3$ of FHA [39].

Similarly, for p orbital, it has energy equal to $n=4$ of FHA. So, for a given ℓ , 1st degenerate SCHA state appears at $n=(\ell+3)$ having energy $-\frac{z^2}{2(\ell+3)^2}$. For a given n , such states can be achieved up to: $\ell=(\ell_{max}-2)=(n-3)$. Therefore, at a fixed n , a given ℓ state contributes as $\frac{(n-\ell-2)(n-\ell-1)}{2}$, giving the total number as,

$$\sum_{\ell=0}^{(n-3)} \frac{(n-\ell-2)(n-\ell-1)}{2} = \frac{n(n-1)(n-2)}{6} \tag{16}$$

(IV) **LCHA:** Similar to CHA, here also a particular ℓ orbital will contribute $(n-\ell-1)$ degenerate states, giving the same total as in CHA, namely, $\sum_{\ell=0}^{(n-1)} (n-\ell-1) = \frac{n(n-1)}{2}$.

Next, we estimate the individual contribution of all four systems in above degeneracy. On the basis of above discussion and following Table I, one can find certain characteristics. To facilitate this, we use n, ℓ to denote principal and orbital quantum number of FHA, whereas n_k, ℓ_j signify the same for other three systems (k, j are integers).

(i) Corresponding to the n th state of FHA, there are $\frac{n(n+1)(n+2)}{6}$ number of degenerate GCHA states, each having the same energy $-\frac{z^2}{2n^2}$.

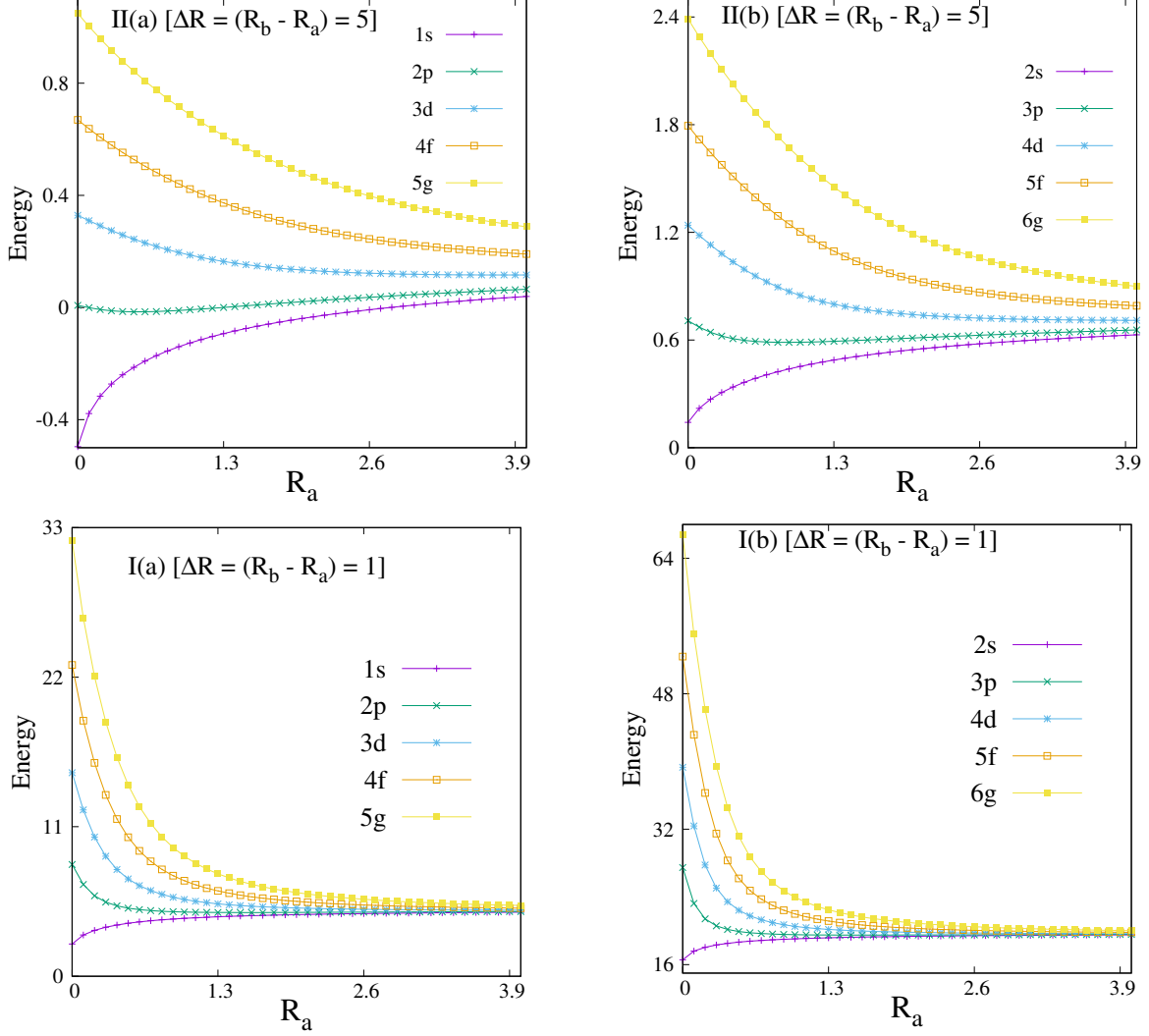


FIG. 1: Energy as function of R_a (in a.u.) in SCHA, for (I) $\Delta R = (R_b - R_a) = 1$ (II) $\Delta R = (R_b - R_a) = 5$. Labels (a), (b), refer to circular and single-node states. See text for details.

- (ii) Each ℓ -state belonging to a certain n , contributes $\frac{(n-\ell)(n-\ell+1)}{2}$ number of GCHA states.
- (iii) Number of incidental degenerate state increases with n . However, at a fixed n , the number of such states reduce with rise in ℓ .
- (iv) The first occurrence of degenerate SCHA state, takes place at $n = 3$.
- (v) At a fixed ℓ , $n_1 < n$. It suggests that, n_1 takes values from $(\ell+1)$ to $n-1$. If we choose $n = 4$, then $\mathcal{E}_4 = -0.03125$. Therefore, for $\ell = 0$, $n_1 = 1, 2, 3$; for $\ell = 1$, $n_1 = 2, 3$; and when $\ell = 2$, $n_1 = 3$.
- (vi) Two arbitrary states (n_1, ℓ_1) , (n_2, ℓ_2) are degenerate when $n_1 < n, \ell_1 < n$ and $n_2 <$

$n, \ell_2 < n$. Note that, they may belong to any of the systems in GCHA, except FHA.

When both R_a, R_b are finite, non-zero, i.e, it is SCHA, the behavior of particle is deeply influenced by R_a, R_b and $\Delta R = (R_b - R_a)$. However, controlling any two parameters would also serve the purpose of the remaining one. It is found that, at a fixed R_b , energy of a given state progresses with R_a (smaller ΔR). Conversely, at a given R_a , a reverse pattern is noticed with rise in R_b (larger ΔR). It is of interest to monitor the energy pattern for a fixed ΔR , with modulations in both R_a and R_b , which is depicted in Fig. 1. The bottom and top panels display energy as a function of R_a at two selected ΔR , namely, 1 and 5 in (I) and (II). The left and right sides record first five circular ($1s, 2p, 3d, 4f, 5g$) and single-node ($2s, 3p, 4d, 5f, 6g$) states, having labels (a), (b). A careful observation reveals that, in either case, energy of $\ell = 0$ states ($1s, 2s$) gradually advances with R_a (squeezing of box). On the contrary, $\ell \neq 0$ states record a decay in the same with growth in R_a ; initially at a quick pace and then slows down until becoming flat at sufficiently large R_a . However, for $\ell > 0$, there is harmony amongst the states with slight differences in lower R_a region.

2. H-plasma

Now, an important question arises: is this special degeneracy a unique feature of one-electron Coulombic systems? To examine it, we extend the calculations on two familiar plasma models: (i) weakly coupled plasma (WCP) or Debye plasma, governed by a potential, $V(r) = -\frac{Z}{r}e^{-\lambda_1 r}$ (ii) exponential cosine screened Coulomb potential (ECSCP), given by, $V(r) = -\frac{Z}{r}e^{-\lambda_2 r} \cos \lambda_2 r$. Here, λ_i is the inverse of Debye radius and represents the interaction between electron and ions in a plasma [72]. In particular, $\lambda_1 = \sqrt{\frac{4\pi e^2 n_e}{k_b T}}$ (n_e, k_b, T signify ion density, Boltzmann constant and plasma temperature respectively), while $\lambda_2 = \frac{k_q}{\sqrt{2}} = \sqrt{\frac{n_e \omega_{pe}}{\hbar}}$ (k_q is the electron plasma wave number connected to plasma frequency and number density). Note that, in WCP, classical interactions are considered, while the quantum effect in a plasma can be added by invoking a $\cos \lambda r$ term in WCP [73]. These two prototypical systems were studied heavily, offering a vast literature. Thus, the influence of screening on energy spectrum [72, 74–76], photo-ionization cross section [77–79], electron-impact excitations [80, 81] were investigated with appreciable interest. Generally speaking, plasma systems have finite number of bound states, which reduces with enhancement of λ .

Let us recall that, in contrast to FHA, the plasma models, WCP and ECSCP are *devoid*

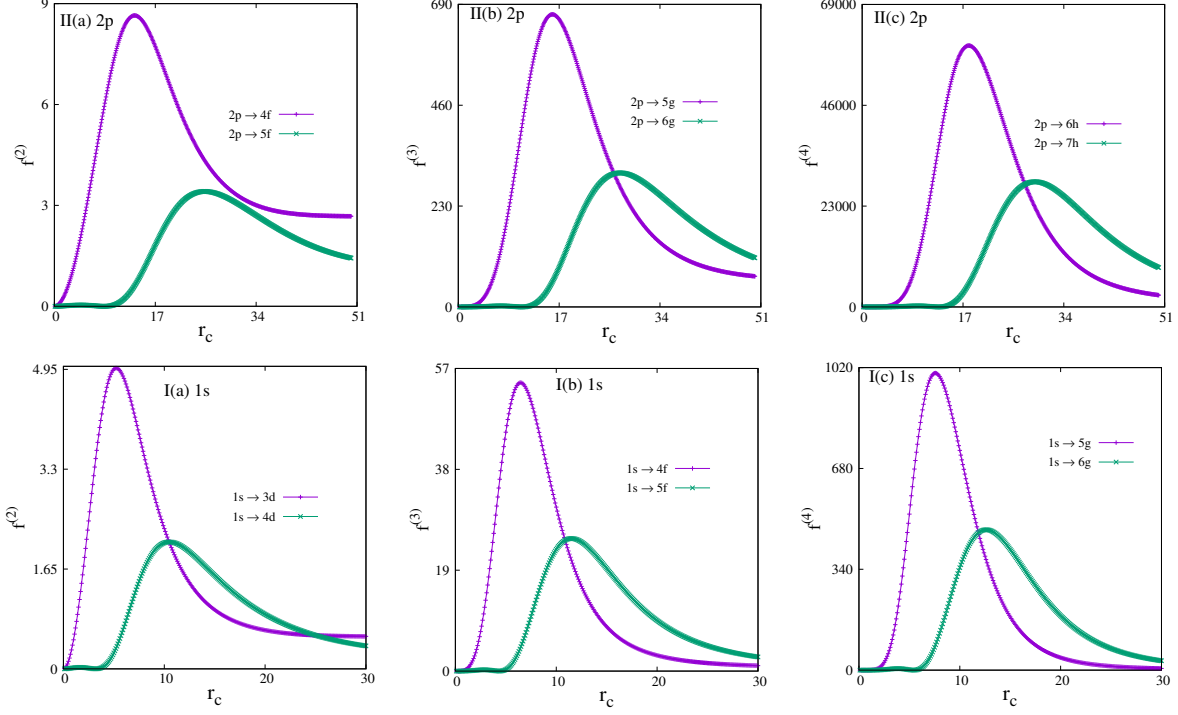


FIG. 2: Plot of $f^{(k)}$ as function of r_c (in a.u.), for (I) $1s$ (II) $2p$ states in CHA. First two transitions are shown; (a), (b), (c) refer to $k = 2, 3, 4$. See text for details.

of accidental degeneracy. Table II illustrates the incidental degeneracy for these, taking $n = 2 - 4$ in s (or $\ell = 0$) states. Like GCHA, here also R_a, R_b are placed at the nodal positions of respective s states in *free* plasmas. In WCP, at $n = 2$ (energy = -0.1152930 a.u.), a three-fold degeneracy exists with one confined ($2a$), one left-confined ($2b$) and one free ($2c$) WCP. This degeneracy in *shell-confined* WCP, however, arises at $n = 3$ with energy -0.04619881 a.u. Thus, at $n = 3$, there survives six degenerate states in *generalized confined* WCP, namely, confined ($3a, 3d$), shell-confined ($3b$), left-confined ($3c, 3e$) and free ($3f$) WCP. Further, at $n = 4$ (energy = -0.0223561 a.u.), there are ten degenerate states belonging to confined ($4a, 4e, 4h$), shell-confined ($4b, 4c, 4f$), left-confined ($4d, 4g, 4i$) and free ($4j$) WCP respectively. Moving to ECSCP system, one encounters exactly identical pattern of degeneracy as WCP, with obvious energy differences between the two. This amply displays the existence of incidental degeneracy in these two plasma systems, implying that such a degeneracy is not necessarily limited to FHA, and may occur in other quantum systems as well. The last two columns represent $\alpha^{(1)}$ and S_r successively. It may be mentioned here that, WCP and ECSCP were invoked to establish the existence of incidental degeneracy in **plasma** potentials. We have not gone beyond this point to undertake an elaborate study of

TABLE III: $f^{(1)}$ values for $1s, 2s, 2p$ states in CHA, SCHA and LCHA. See text for details.

R_a	R_b	$1s \rightarrow 2p$	$1s \rightarrow 3p$	$2s \rightarrow 2p$	$2s \rightarrow 3p$	$2p \rightarrow 1s$	$2p \rightarrow 2s$	$2p \rightarrow 3d$	$2p \rightarrow 4d$
0	1	0.98455839	0.00772592	-0.60825789	1.56032656	-0.32818613	0.20275263	1.08482483	0.01857681
0.1	1	0.89910222	0.09117798	-0.54875155	1.26759877	-0.29970074	0.18291718	1.07826147	0.02579334
0.2	1	0.81158829	0.17664462	-0.46434643	1.01215223	-0.27052943	0.15478214	1.04448022	0.05966553
0.5	1	0.69746119	0.28964404	-0.35084205	0.73447901	-0.23248706	0.11694735	0.92955029	0.17316032
0.8	1	0.66991458	0.31699958	-0.32345071	0.67370461	-0.22330486	0.10781690	0.89321899	0.20918396
0	2	0.99105877	0.00000217	-0.61189926	1.57832558	-0.33035292	0.20396642	1.09062730	0.01308847
0.1	2	0.96414685	0.02875100	-0.60923016	1.46958646	-0.32138228	0.20307672	1.08969744	0.01424386
0.5	2	0.78114997	0.20643653	-0.43425912	0.93184418	-0.26038332	0.14475304	1.02245081	0.08147398
1	2	0.69749557	0.28958819	-0.35086313	0.73452648	-0.23249852	0.11695438	0.92959980	0.17310450
1.2	2	0.68355578	0.30344579	-0.33700278	0.70354791	-0.22785193	0.11233426	0.91134321	0.19119914
1.5	2	0.67205870	0.31486957	-0.32557999	0.67836486	-0.22401957	0.10852666	0.89607618	0.20634732
1.8	2	0.66739177	0.31950490	-0.32094504	0.66823564	-0.22246392	0.10698168	0.88985569	0.21252327
0	5	0.84879929	0.10827497	-0.45637469	1.42333674	-0.28293310	0.15212490	1.10303346	0.00102259
1	5	0.82132944	0.16452278	-0.47393100	1.02743235	-0.27377648	0.15797700	1.05560747	0.04906997
2	5	0.72015051	0.20643653	-0.37324792	0.78555850	-0.24005017	0.12441597	0.95825952	0.14467096
2.5	5	0.69759377	0.28958819	-0.35089758	0.73466209	-0.23253126	0.11696586	0.92974209	0.17292899
3	5	0.68357365	0.30344579	-0.33700060	0.70357230	-0.22785788	0.11233353	0.91136832	0.19116227
4	5	0.66991478	0.31486957	-0.32344989	0.67370488	-0.22330493	0.10781663	0.89321926	0.20918302
4.5	5	0.66739177	0.31950490	-0.32094500	0.66823564	-0.22246392	0.10698167	0.88985569	0.21252323
0	10	0.49203980	0.25817376	-0.07781857	0.96754959	-0.16401327	0.02593952	1.07006404	0.02801599
0.5	10	0.97045316	0.01437069	-0.62098640	1.56331874	-0.32348439	0.20699547	1.08623978	0.01685871
1	10	0.94767400	0.02402487	-0.58992446	1.36743381	-0.31589133	0.19664149	1.10659524	0.00041483
2	10	0.82883015	0.14973954	-0.47587757	1.03956806	-0.27627672	0.15862586	1.06686692	0.03701308
3	10	0.75955649	0.22459445	-0.41041279	0.87499038	-0.25318550	0.13680426	1.00438637	0.09839538
5	10	0.69774060	0.28903455	-0.35085740	0.73486495	-0.23258020	0.11695247	0.92995783	0.17260954
7	10	0.67494769	0.31198282	-0.32843445	0.68465713	-0.22498256	0.10947815	0.89992293	0.20251950
9.5	10	0.66683858	0.32005426	-0.32039568	0.66703853	-0.22227953	0.10679856	0.88911811	0.21325570
0	∞	0.41619672	0.07910156	0.00000000	0.43486544	-0.13873224	0.00000000	0.69578470	0.12179511
0.1	∞	0.61261825	0.08716313	-0.27197479	0.76653089	-0.20420608	0.09065826	0.69643208	0.12177348
0.5	∞	0.91228737	0.03992888	-0.50501203	1.34020061	-0.30409579	0.16833734	0.73703538	0.11966976
1	∞	0.95710827	0.00509331	-0.46634518	1.42628570	-0.31903609	0.15544839	0.84505124	0.10660158
2	∞	0.91518127	0.00537086	-0.38224386	1.32047405	-0.30506042	0.12741462	1.01517164	0.05572610
5	∞	0.82683246	0.05128960	-0.29816602	1.10002016	-0.27561082	0.09938867	1.08031802	0.00001907
7	∞	0.79907239	0.07217889	-0.27883906	1.02880135	-0.26635746	0.09294635	1.05975869	0.00511577
8	∞	0.78916499	0.08038843	-0.27256657	1.00309177	-0.26305500	0.09085552	1.04975557	0.00959527
9	∞	0.78094995	0.08751295	-0.26761185	0.98164753	-0.26031665	0.08920395	1.04067662	0.01429067
10	∞	0.77400929	0.09376540	-0.26360162	0.96343656	-0.25800310	0.08786721	1.03254711	0.01891643

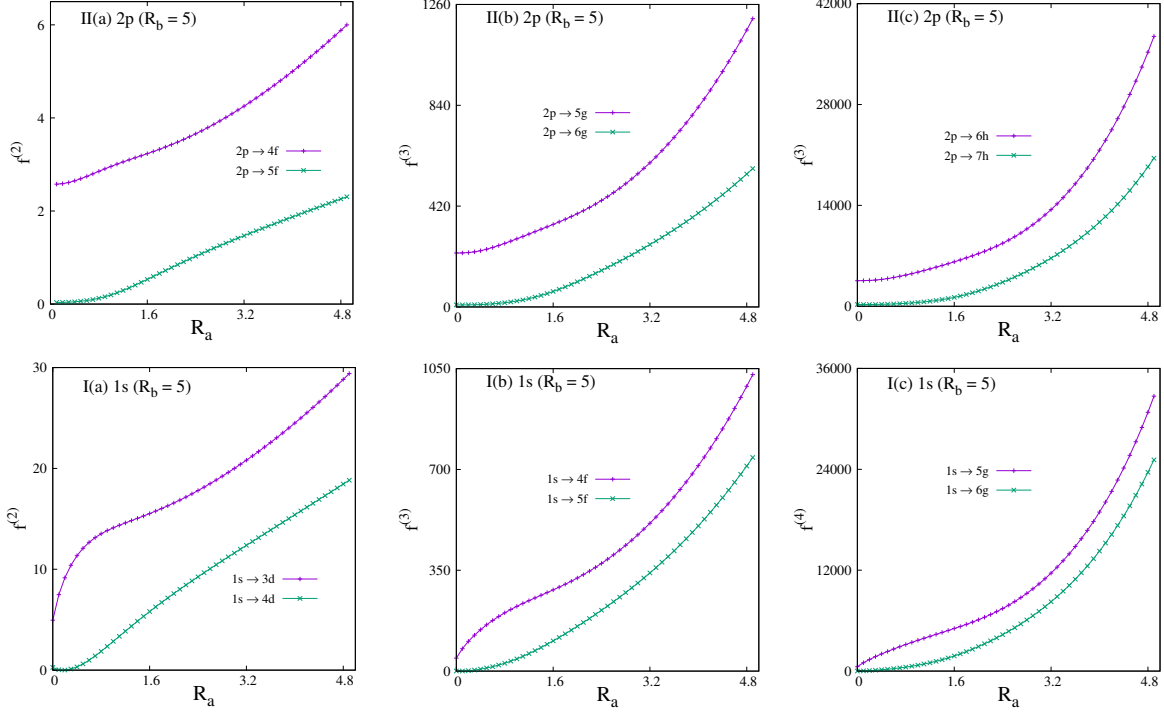


FIG. 3: Plot of $f^{(k)}$ as function of R_a (in a.u), keeping R_b fixed at 5, for (I) $1s$ (II) $2p$ states in SCHA. First two transitions are shown; (a), (b), (c) refer to $k = 2, 3, 4$. See text for details.

incidental degeneracy in these two **or other** systems and may be explored in future.

B. Multipole oscillator strength and polarizability

Unlike the previous section on energy, here we have split the discussion of $f^{(k)}$ and $\alpha^{(k)}$ ($k = 1 - 4$) on confined H-like ions and its *free* counterpart, in some low-lying states. Except $\alpha^{(1)}$ of $1s$ in SCHA, no such results are reported so far in any other GCHA model. Wherever possible, these are compared with available literature. As an offshoot, analytical closed-form expression of $f^{(k)}$ and $\alpha^{(k)}$ (considering the bound-state contribution) are **presented in Appendix A for $k = 1, 2, 3, 4$, in case of FHA.**

At the outset, we note that, the oscillator strength sum rule, Eq. (9) is verified for all states in CHA, SCHA, LCHA, for $k = 1 - 4$. By definition, $f^{(k)}$ determines the probability of transition from an initial to a final state. For absorption/emission, it is (+)ve/(-)ve.

The selection rule for $f^{(1)}$ is $\Delta\ell = \pm 1$. Note that, from an s state, transition can take place only to a p state. However, from p , transition can happen to both s and d states. Table III imprints calculated $f^{(1)}$ for $1s, 2s, 2p$ for $n, \ell \rightarrow n', (\ell + 1)$ ($n = 1, 2; n' = 2, 3, 4$)

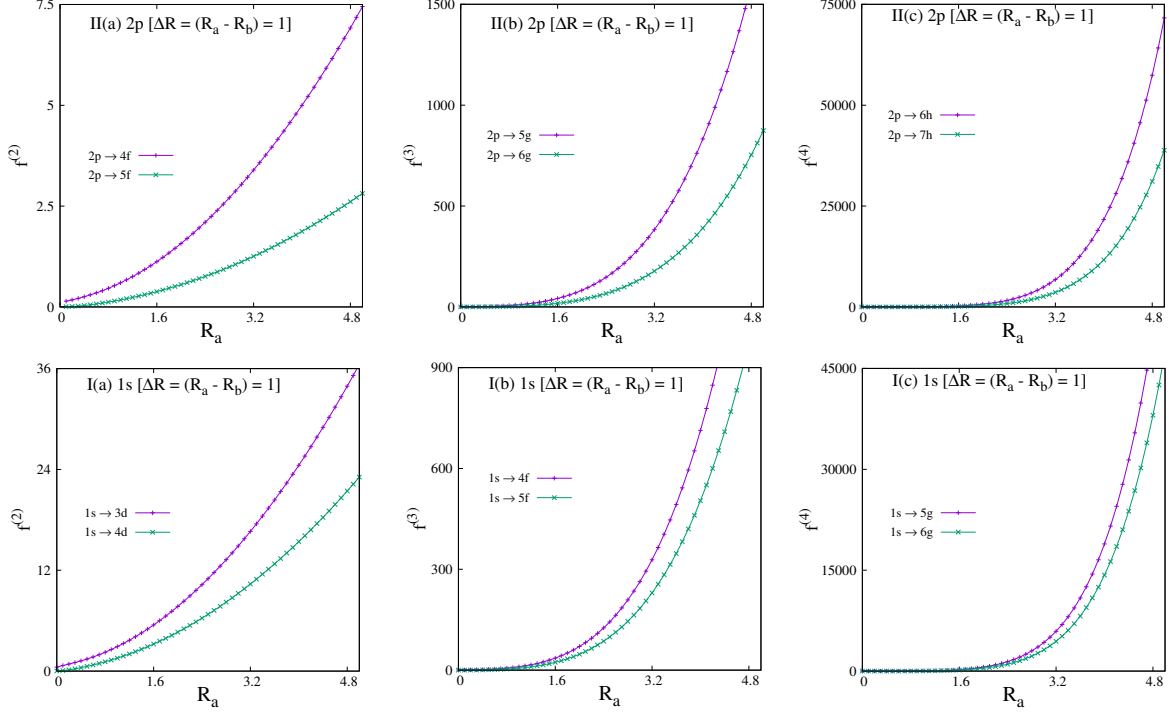


FIG. 4: Plot of $f^{(k)}$ (in a.u.) as function of R_a , for $\Delta R = (R_b - R_a) = 1$ in (I) $1s$ (II) $2p$ states in SCHA. First two transitions are shown; (a), (b), (c) refer to $k = 2, 3, 4$. See text for details.

transitions. In this context, SCHA results are offered for four R_b , namely, 1, 2, 5, 10; for each R_b , R_a lies in between $0 - R_b$. The bottom part shows results for LCHA, having ten separate R_a (including 0, leading to the special case of FHA), for $R_b = \infty$. Further, one recovers a CHA situation when $R_a = 0$, while $r_c = R_b = 1, 2, 5, 10$. It is noticed that, $f_{1s \rightarrow 2p}^{(1)}$ in CHA increases with r_c to attain a maximum, and then falls down to merge to FHA. In SCHA, for $R_b \leq 5$, it decreases with rise in R_a ; but at $R_b = 10$, it slowly reaches a maximum before finally declining. On the contrary, in LCHA, it grows with R_a to attain a maximum, and then decays down. The behavior of $f_{1s \rightarrow 3p}^{(1)}$ is, however, somehow different from $f_{1s \rightarrow 2p}^{(1)}$, e.g., a reverse trend is recorded in case of CHA; however, at $r_c \rightarrow \infty$, eventually it converges to FHA. In SCHA, the pattern generated for a given R_b for various R_a , generally differs with change in R_b . However, in LCHA it travels through a maximum, then a minimum and again rises. In case of $2s \rightarrow 2p$ transition, $f^{(1)}$ is always (-)ve, which implies that, except FHA (where they are degenerate), the former has higher energy than latter. As usual, in CHA $f_{2s \rightarrow 2p}^{(1)}$ approaches the FHA limit for $R_a \rightarrow 0, R_b \rightarrow \infty$. In SCHA, at $R_b = 1$ (and 2), it enhances with R_a , but for $R_b = 5$ (and 10), it reaches a minimum and then advances. A similar pattern is also noticed in LCHA for $R_b = 5$ (and 10). In case of $2s \rightarrow 3p$ transition,

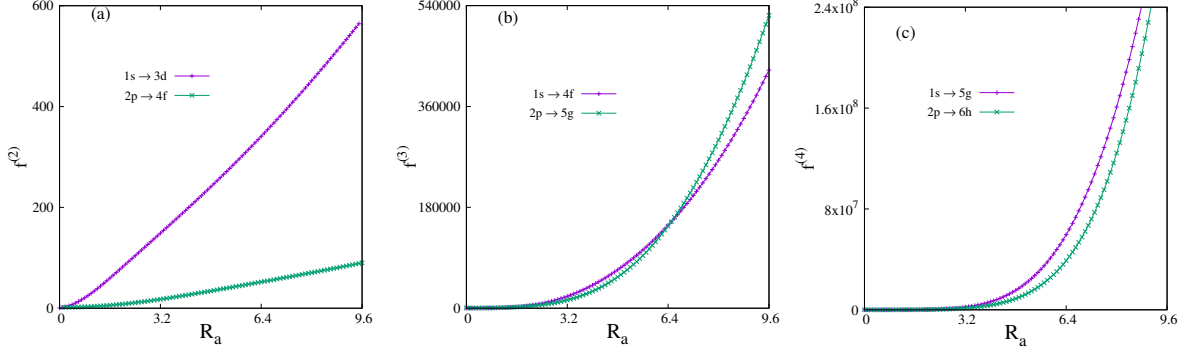


FIG. 5: Plot of $f^{(k)}$ (in a.u.) as function of R_a for $1s$ and $2p$ states in LCHA. Panels (a), (b), (c) refer to $k = 2, 3, 4$. See text for details.

$f^{(1)}$ in CHA and LCHA imprint resembling nature, i.e., decays after attaining a maximum. But the trend in SCHA differs from $R_b \leq 5$ (falls as R_a progresses). At $R_b = 10$, a reverse trend is recorded. In contrast to $1s$ and $2s$, the behavior of $f^{(1)}$ in $2p$ is not straightforward. Nevertheless, a few comments can be made: (i) at $r_c \rightarrow \infty$ limit, CHA results converge to FHA (ii) $f^{(1)}$ in SCHA (at $R_b = 10$) and LCHA display analogous character. Though in respective cases this pattern alters. (iii) $f_{2p \rightarrow 3d}^{(1)}$ and $f_{2p \rightarrow 4d}^{(1)}$ show opposite features.

Now, the focus is on higher order $f^{(k)}$, for which results are depicted graphically in case of $k = 2 - 4$, related to *quadrupole*, *octupole* and *hexadecapole* transitions. Corresponding selection rules are: $\Delta\ell = 0, \pm 2$, $\Delta\ell = \pm 1, \pm 3$ and $\Delta\ell = 0 \pm 2, \pm 4$ respectively. In Fig. 2, bottom (I) and top (II) rows represent transitions from $1s$ and $2p$ states, for the respective maximum $\Delta\ell$ values, having $k = 2, 3, 4$, in panels designated as (a), (b), (c). For each k first two transitions from these two states are exhibited in terms of $f^{(k)}$ versus r_c in CHA. In case of $1s \rightarrow (3d, 4f, 5g)$ and $2p \rightarrow (4f, 5g, 6h)$ transitions, respective $f^{(k)}$'s pass through a distinct maximum. But for remaining six transitions, *viz.*, $1s \rightarrow (4d, 5f, 6g)$ and $2p \rightarrow (5f, 6g, 7h)$, there appears a shallow maximum followed by a prominent one. Figure 3 now exhibits variation of $f^{(2)}, f^{(3)}, f^{(4)}$ in left, middle and right panels, as function of R_a in SCHA keeping R_b stationary at 5. The same two states generating same transitions of previous table are considered. In this instance, $f^{(k)}$ always advances with R_a . Figure 4 plots $f^{(k)}$ against R_a , keeping $\Delta R = (R_b - R_a)$ fixed at 1, in SCHA. The presentation strategy is similar to that in Figs. 2 and 3. In all occasions, $f^{(k)}$'s progress with R_a . Likewise, Fig. 5 depicts $f^{(2)}$ for $1s \rightarrow 3d, 2p \rightarrow 4f$; $f^{(3)}$ for $1s \rightarrow 4f, 2p \rightarrow 5g$; and $f^{(4)}$ for $1s \rightarrow 5g, 2p \rightarrow 6h$, transitions in LCHA, in panels (a)-(c). One finds that, like the previous figure, here also

$f^{(k)}$'s grow with R_a ; the y-axis dramatically increases, as k goes from 2 to 4.

Now we move to investigate $\alpha^{(1)}$ in GCHA by means of sample calculations on $1s, 2s, 2p, 3s, 3d, 4s$ states. For p and d states, allowed transitions occur to final states having ℓ as $(0, 2)$ and $(1, 3)$ respectively. The collected results in Table IV include contributions from both ℓ , for same numerical values of R_a, R_b of previous table. The third column provides the volume of ring ($V = R_b^3 - R_a^3$) having inner and outer radii R_a, R_b . Note that, $(R_a, R_b) = (0, 1), (0, 2), (0, 5), (0, 10)$ represent CHA cases. LCHA results are tabulated in the bottom segment, while its first row correspond to a FHA. Some of these for CHA and SCHA were reported in [3], which are duly quoted in footnote. Our calculated $\alpha^{(1)}$ values show excellent agreement with these. A careful analysis of this table uncovers several interesting features, some of which are enumerated below:

1. **CHA:** In FHA, $\alpha^{(1)}$ is a (+)ve quantity. At a given ℓ , it rises in n , while, at a fixed n , it progresses with ℓ . However, in CHA, the pattern behavior is not so consistent, recording distinct changes with r_c , offering both (+)ve and (-)ve values. A straightforward inference is that, with growth in r_c , $\alpha^{(1)}$ in a given state with an arbitrary ℓ progresses as r_c proceeds towards the respective FHA limit. At $r_c = 2, 5, 2s, 3s, 4s$ states offer (-)ve polarizability; the same is also found for latter two states at $r_c = 10$.
2. **SCHA:** In this situation, characteristics of $\alpha^{(1)}$ changes with ℓ . For s -wave states, (at a fixed R_b) it increases with R_a . A resembling nature in $\alpha^{(1)}$ is also achieved by varying R_b keeping R_a fixed. These two outcomes suggest that, it depends on (R_a, R_b) pair, but not on their difference, ΔR . On the contrary, for $\ell \neq 0$ states, at a specific R_b , it abates with R_a , but for a given R_a , it advances with R_b . Thus, in this scenario, $\alpha^{(1)}$ is controlled by all three quantities, $R_a, R_b, \Delta R$.

3. **LCHA:** In $\ell = 0$ states, it grows with R_a , but a *zigzag* pattern is seen for $2p$ and $3d$.

It is observed from Table IV that, for s -waves, at a fixed R_b , $\alpha^{(1)}$ progresses with R_a . However, after some characteristic R_a , it prevails over volume, given in third column. According to *Herzfeld criterion* [3, 83] insulator \rightarrow metal conversion occurs under the condition,

$$\frac{4\pi}{3}V \leq \left(\frac{4\pi}{3}\right) \alpha^{(1)}, \quad V = (R_b^3 - R_a^3) \leq \alpha^{(1)}. \quad (17)$$

Now, applying the above criterion, one can easily discern that, in SCHA metallic character can be observed in all the s states. This feature was reported before [3] in the *ground state* of

TABLE IV: $\alpha^{(1)}$ values for $1s, 2s, 3s, 4s, 2p, 3d$ states in GCHA. See text for details.

R_a	R_b	V	$\alpha_{1s}^{(1)}$	$\alpha_{2s}^{(1)}$	$\alpha_{3s}^{(1)}$	$\alpha_{4s}^{(1)}$	$\alpha_{2p}^{(1)}$	$\alpha_{3d}^{(1)}$
0	1	1	0.02879202 [†]	0.00441401	0.00188747	0.00105362	0.01715126	0.00894345
0.1	1	0.999	0.04759422 [†]	0.02720296	0.02357306	0.02219162	0.01004334	0.00815930
0.2	1	0.992	0.07284697 [†]	0.05487311	0.05124972	0.04988689	0.00583028	0.00565908
0.5	1	0.875	0.20188347 [†]	0.19133640	0.18923265	0.18848057	0.00083203	0.00083480
0.8	1	0.488	0.43528355	0.43282926	0.43236928	0.43220786	0.00002109	0.00002109
0	2	8	0.34255811 [‡]	-0.0168850	-0.00436115	-0.00163080	0.30828166	0.15185462
0.1	2	7.999	0.51258523 [‡]	0.22332074	0.19042816	0.17549582	0.21885819	0.149192555
0.5	2	7.875	1.37743250 [‡]	1.14984366	1.09461376	1.07278640	0.07037524	0.07079627
1	2	7	3.22129727 [‡]	3.0635182	3.02914678	3.01659244	0.01330690	0.01335487
1.2	2	6.272	4.25881264	4.1404792	4.11614071	4.10740597	0.00542262	0.00542936
1.5	2	4.625	6.20198032	6.1449042	6.13390400	6.13002002	0.00082430	0.00082441
1.8	2	2.168	8.67861281	8.6676719	8.66563354	8.66491917	0.00002106	0.00002108
0	5	125	3.42245422	-21.10657309	-5.69164044	-2.65407833	18.08924616	7.21196971
1	5	124	38.3097689	34.92837261	32.75186815	31.71727294	3.57857074	3.72434520
2	5	117	90.3835855	85.34545419	83.48828979	82.73474712	1.08353807	1.09660163
2.5	5	109.375	124.798441	119.92301897	118.49342276	117.94158361	0.51897086	0.52129425
3	5	98	165.908991	161.85822945	160.86291102	160.49304359	0.21171092	0.21200753
4	5	61	272.010054	270.53059396	270.23821589	270.13447254	0.01317982	0.01318049
4.5	5	33.875	339.006228	338.58155287	338.50168038	338.47363247	0.0008232	0.00082310
0	10	1000	4.49681419 [§]	37.23973625	-376.86905909	-143.24860953	793.3231266	171.8366872
0.5	10	999.875	57.8605712	87.17950256	107.31693132	110.54059768	107.3856268	152.9035064
1	10	999	163.642519	277.6753968	254.03479328	238.63416165	80.69486982	113.7656686
2	10	992	485.283240 [§]	583.9858189	540.82756495	518.84632115	52.316849	60.8621082
3	10	973	900.888347 [§]	936.7193051	895.52440838	876.03156272	31.4884761	33.2715571
5	10	875	1969.35287 [§]	1925.755087	1900.38211125	1889.89454238	8.2726984	8.32191160
7	10	657	3430.37098 [§]	3390.605514	3380.46513160	3376.69265692	1.0688590	1.06926410
9.5	10	142.625	6023.026447	6021.229170	6020.89385098	6020.77626011	0.0008310	0.000836
0	∞	-	4.50000000 [±]	120.0000000 [±]	1012.5000000 [±]	4992.0000000 [±]	176.0000000 [±]	1863.0000000 [±]
0.1	∞	-	11.0436170	-832.82391	-19470.0124	-157741.0999	551.13773744	1862.6259940
0.5	∞	-	62.0058551	1191.23431	6853.5900	20163.4888	300.6834286	24243.2503
1	∞	-	206.890953	3978.47424	29050.9501	131865.02	311.4948323	7601.124077
2	∞	-	928.385427	13601.4303	89661.9116	389708.7	466.836635	3831.84946
5	∞	-	10180.1611	90653.1600	458038.2	1685829.4	1425.94246	3701.13787
7	∞	-	27077.8811	199530.231	900453.4	-	2448.04066	4859.03373
8	∞	-	40427.5127	276691.870	-	-	3080.4164	5613.81181
9	∞	-	57889.5118	371559.069	1538454.7	-	3797.0113	6473.34645
10	∞	-	80147.5187	486116.385	1941232.3	-	4600.2812	7434.64009

[†]Literature results [3] for $\alpha_{1s}^{(1)}$ ($R_b = 1$) at $R_a = 0, 0.1, 0.2, 0.5$ are: 0.0284, 0.0473, 0.0716, 0.2000.

[‡]Literature results [3] for $\alpha_{1s}^{(1)}$ ($R_b = 2$) at $R_a = 0, 0.1, 0.5, 1.0$ are: 0.3405, 0.5095, 1.3588, 3.2041.

[§]Literature results [3] for $\alpha_{1s}^{(1)}$ ($R_b = 10$) at $R_a = 0, 2, 3, 5, 7$ are: 4.4851, 474.3865, 880.0750, 1962.3385, 3394.0953.

[±]Literature results [82] for $\alpha_{1s}^{(1)}, \alpha_{2s}^{(1)}, \alpha_{3s}^{(1)}, \alpha_{4s}^{(1)}, \alpha_{2p}^{(1)}, \alpha_{3d}^{(1)}$ in FHA are: 4.5, 120, 1012.5, 4992, 176, 1863.

TABLE V: Estimated $R_a = R_m$ at ten R_b , for $1s, 2s, 3s, 4s$ states in SCHA. See text for details.

R_b	$R_a = R_m$			
	$1s$	$2s$	$3s$	$4s$
1	0.81776350	0.81844574	0.818572206	0.818616480
2	1.380547989 [†]	1.386963908	1.388196667	1.388631630
3	1.78705451 [†]	1.806803958	1.810946733	1.812435703
4	2.091846379 [†]	2.130115046	2.139377180	2.1427985178
5	2.329536517 [†]	2.385985164	2.40275065	2.4091529423
6	2.524110980 [†]	2.591789087	2.618502823	2.629078449
7	2.692788378 [†]	2.758505970	2.7976385904	2.813701635
8	2.847829929 [†]	2.893365851	2.9474474821	2.9704167040
9	2.997651615 [†]	3.00123877	3.0729537329	3.104343080
10	3.147719215 [†]	3.08540221	3.177732377	3.219149730

[†]For $R_b = 2, 3, 4, 5, 6, 7, 8, 9, 10$, literature results [3] of R_m are: 1.73, 2.08, 2.34, 2.54, 2.71, 2.87, 3.01, 3.15, 3.29 respectively.

SCHA. This work, however, shows that, it can be extended to excited states as well having $\ell = 0$. The threshold R_a at which $\alpha^{(1)}$ surpasses V (symbolized as R_m), is produced in Table V, for four s states, at ten selected R_b (1, 2, 3, 4, 5, 6, 7, 8, 9, 10). For a given $\alpha^{(1)}$, R_m tends to assume larger values with growth of R_b . Moreover, with an enhancement of R_b , the metallic zone ($R_b - R_m$) extends. The lone reference results are quoted in the footnote, which shows decent qualitative agreement.

Now we present a cross section of results on 2^k -pole polarizabilities ($k = 2, 3, 4$) of $1s$ state in CHA, SCHA and LCHA graphically in Fig. 6. The left (a), middle (b) and right (c) panels represent these for quadrupole, octupole and hexadecapole polarizabilities. The bottom row (I) for CHA indicates, for all k , $\alpha^{(k)}$ sharply increases with r_c , before finally merging to the respective FHA limit. Parallel results for SCHA against R_a are depicted in panels marked (II), while keeping R_b fixed at 5—reflecting a steady monotonic growth. Similarly panels III(a), III(b), III(c) offer SCHA results varying both R_a, R_b , maintaining a constant $\Delta R = 1$. However here also the monotonic increasing trend is maintained for all k , as in previous SCHA situation. At last, the top-most panels IV(a), IV(b) and IV(c) show the respective plots in case of LCHA, bearing a close resemblance to SCHA scenario.

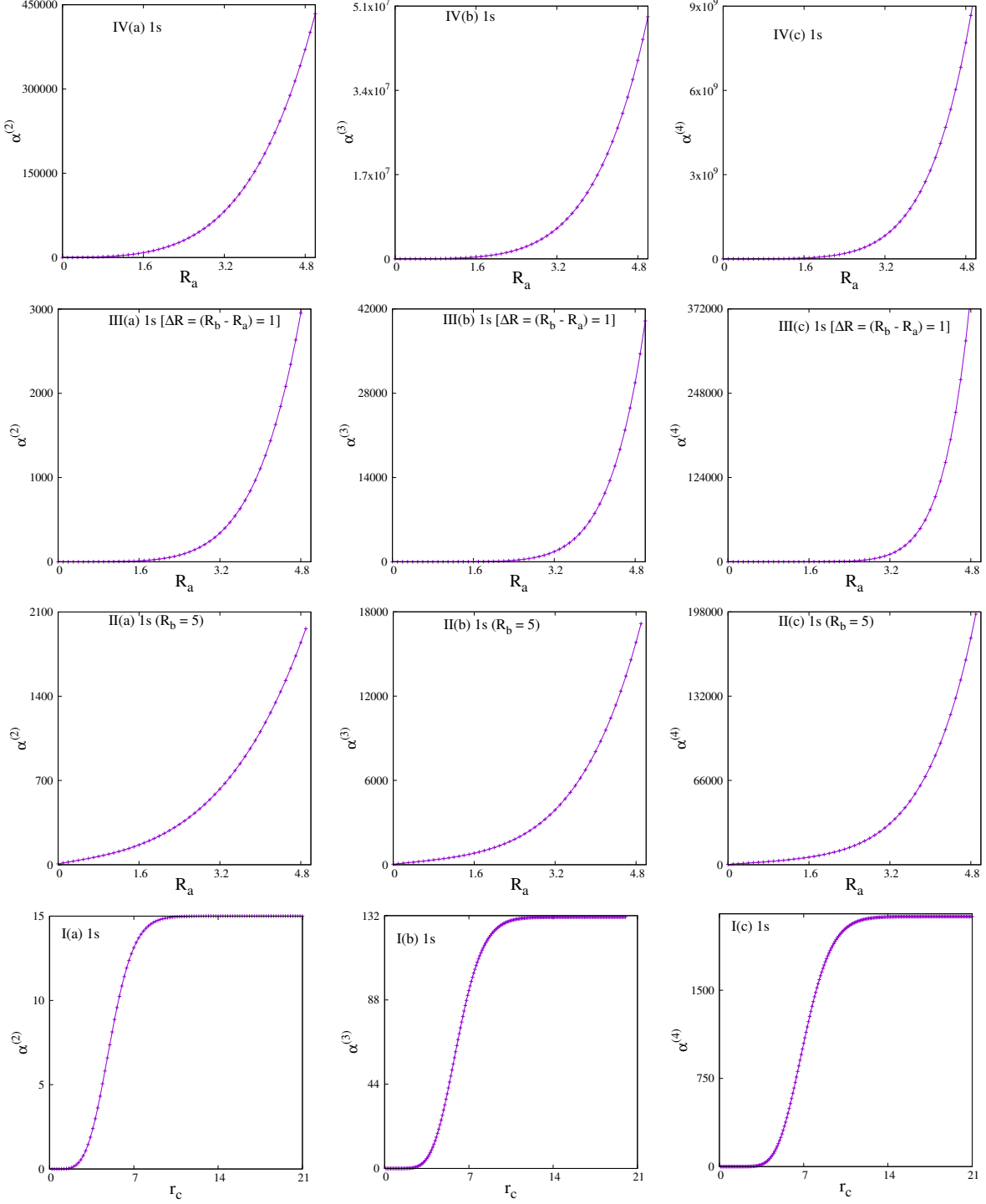


FIG. 6: Plot of $\alpha^{(k)}$ ($k = 2 - 4$), in panels (a)-(c) in 1s state in GCHA. In CHA (I) they are plotted as function of r_c (in a.u.). In (II) and (IV) they are shown against R_a for SCHA and LCHA. In (III), these are given, for SCHA, considering $\Delta R = (R_b - R_a) = 1$. See text for details.

C. Information entropy

Now we will present some results on information entropy. A few points are worth noting before that. The net information measure in r and p space in a central potential, may be separated into two parts, *viz.*, (i) radial and (ii) angular contributions, as mentioned in Eq. (10). The latter remains unchanged in two conjugate spaces in these systems; furthermore, the same is true for different confinement situations of GCHA, modelled by various boundary conditions. Moreover, we have opted magnetic quantum number m as 0, unless stated otherwise. In all reported cases, $S_{\mathbf{r}} + S_{\mathbf{p}} = S_t$ satisfy the lower bound: $3(1 + \ln \pi)$.

Representative $S_{\mathbf{r}}$ and $E_{\mathbf{r}}^O$ for $1s$ state in GCHA are tabulated in Table VI. The SCHA results provided at four R_b (1, 2, 5, 10) shows that $S_{\mathbf{r}}$ progresses with R_a to reach a plateau and then declines. That means, for each R_b , there is a range of R_a , where $S_{\mathbf{r}}$ grows with decrease in ΔR . However, the changes in $S_{\mathbf{p}}$ is not so straightforward. At $R_b = 1$, it increases with rise in R_a , while at $R_b = 2, 5$ or 10, it passes through a shallow minimum. Thus, with reduction in shell radius (ΔR), $S_{\mathbf{r}}, S_{\mathbf{p}}$ increases and decreases, signifying a gain and loss in uncertainty in r and p spaces. This is a reverse trend to what is observed in CHA [25], where a shortening of r_c , causes fall and rise in $S_{\mathbf{r}}$ and $S_{\mathbf{p}}$. However, at a fixed R_a , their sum, $S_{\mathbf{r}} + S_{\mathbf{p}} = S_t$ always advances with growth of R_b . As usual, $E_{\mathbf{r}}^O, E_{\mathbf{p}}^O$ portray opposite trend with respect to $S_{\mathbf{r}}, S_{\mathbf{p}}$. At a fixed R_b , $E_{\mathbf{r}}^O$ collapses to a flat minimum and $E_{\mathbf{p}}^O$ rises up to a shallow maximum. Moreover, E_t^O always declines with rise in R_a . This pattern complements the outcome of S . The bottom segment provides results for LCHA. Unlike SCHA, here the trend of $S_{\mathbf{r}}$ and $S_{\mathbf{p}}$ very candid; with growth in R_a , former enhances, while latter declines. On the contrary, $E_{\mathbf{r}}^O$ reduces and $E_{\mathbf{p}}^O$ advances with change in R_a . Further, S_t decays to reach a shallow minimum and E_t^O approaches to a flat maximum.

The above results of SCHA and LCHA in ground state drives us to extend the study in $\ell \neq 0$ states. Thus, we present $S_{\mathbf{r}}$ for first five circular (node-less) states in SCHA and LCHA in Fig. 7. The three rows I, II, III, from bottom to top correspond to SCHA, SCHA having a fixed $\Delta R = 1$ and LCHA; $\ell = 0-4$ states are given labels (a)-(e). Like the previous plots of $f^{(k)}$ and $\alpha^{(k)}$, here also, SCHA graphs are presented in two separate forms. At first, $S_{\mathbf{r}}$ is plotted against R_a keeping R_b fixed at 5 in bottom row panels I. In $1s$, a distinct dome-shaped structure appears, while for remaining states, the initial shape is partially lost retaining the sharp decay at large R_a . Secondly, in middle row panels marked II, $S_{\mathbf{r}}$ is shown

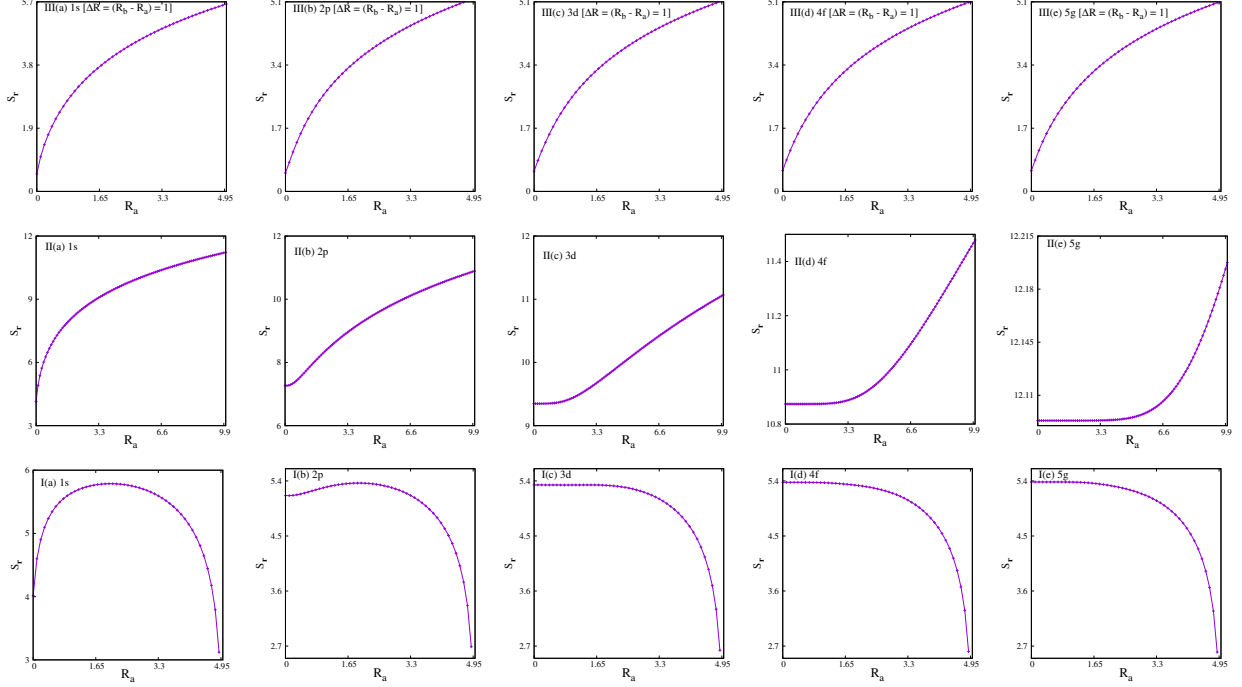


FIG. 7: Plot of S_r as function of R_a (in a.u.) for $1s, 2p, 3d, 4f, 5g$ states in (I) SCHA ($R_b = 5$) (II) SCHA, keeping ΔR fixed at 1 a.u. (III) LCHA. Consult text for details.

as function of R_a keeping ΔR constant at 1. In all five states S_r firmly progresses with R_a . The top row marked III, displays the respective plot for LCHA. In $1s$ (panel (a)), it grows uninterruptedly. For other states, in the beginning, there is a resistance to change. In other words, it remains invariant up to a certain R_a , and then enhances.

IV. FUTURE AND OUTLOOK

Incidental degeneracy, multipole oscillator strength, multipole polarizability, Shannon entropy and Onicescu **information** energy have been investigated for GCHA model, with special emphasis on SCHA, which has not been done before. The proposed model can explain both *free* and *confined* systems effectively. An in-depth analysis reveals several fascinating and hitherto unreported features in such systems. The possibility of this degeneracy in Debye and exponential-cosine screened plasma environment has been established. In GCHA with increase in n number of these degenerate states increases, while at a fixed n , with growth in ℓ , their count declines. In confined condition, *negative* polarizability is encountered in ground and several excited states, which in accordance with Herzfeld criterion, suggests metallic character. Simplified analytical expressions of $f^{(k)}, \alpha^{(k)}$ in FHA are reported. The impact

TABLE VI: S and E^O for ground state in GCHA. See text for details.

R_a	R_b	S_r	S_p	$S_t = S_r + S_p$	E_r^O	E_p^O	$E_t^O = E_r^O E_p^O$
0	1	0.52903053	6.0114	6.5404	0.84791729	0.00364537	0.00309098
0.1	1	0.77666759	6.040785	6.817452	0.56908172	0.004180	0.002378
0.2	1	0.89751313	6.23932	7.13683	0.47934610	0.004133	0.001981
0.5	1	0.93965484	7.35022	8.28987	0.43687955	0.0025784	0.0011264
0.8	1	0.40237874	9.9389	10.3412	0.73903793	0.00056417	0.00041694
0	2	2.39666961	4.09171	6.48837	0.14785297	0.0254120	0.0027572
0.1	2	2.66321083	3.93985	6.60306	0.09448635	0.030017	0.002836
0.5	2	3.00050972	4.30210	7.30261	0.05789843	0.03171950	0.00183651
1	2	3.01785556	5.28370	8.30155	0.05469677	0.020779	0.001136
1.2	2	2.93197744	5.88332	8.81529	0.05923939	0.014951	0.000885
1.5	2	2.64748816	7.20552	9.85300	0.07834727	0.0068029	0.0005329
1.8	2	1.89807736	9.88472	11.78280	0.16543757	0.00124238	0.0002055
0	5	4.01744418	2.5243610	6.5418051	0.04217574	0.16706123	0.00704593
1	5	5.63473499	1.4621	7.0968	0.00432817	0.490356	0.002122
2	5	5.78652038	2.06176	7.84828	0.00347700	0.404385	0.001406
2.5	5	5.76289185	2.52188	8.28477	0.00351784	0.321734	0.001131
3	5	5.67961160	3.12263	8.80224	0.00379731	0.231656	0.000879
4	5	5.23062327	5.0882	10.3188	0.00591282	0.071235	0.000421
4.5	5	4.64694680	7.1204	11.7673	0.01058804	0.01925812	0.00020390
0	10	4.14461075	2.42193665	6.5665474	0.03978966	0.20886414	0.00831063
0.5	10	6.22396712	0.317019	6.540986	0.00339560	1.3629551	0.00462805
1	10	6.96632717	-0.31664	6.64968	0.00140630	2.47609	0.00348
2	10	7.56814293	-0.5044	7.0637	0.00065283	3.5697296	0.0023304
3	10	7.77837713	-0.3423	7.4360	0.00049254	3.621882	0.001783
5	10	7.83556437	0.4567	8.2922	0.00044356	2.561340	0.001136
7	10	7.59776142	1.8617	9.4594	0.00055562	1.154784	0.000641
9.5	10	6.08547241	7.057	13.142	0.00251172	0.040427	0.000101
0	∞	4.14472988	2.42186234	6.56659222	0.03978873	0.20897494	0.00831484
0.1	∞	4.90515587	1.6122737	6.51742957	0.01564470	0.41905958	0.01912784
0.5	∞	6.26312315	0.28264261	6.54576576	0.00333958	1.48254647	0.00495108
1	∞	7.15077757	-0.521160	6.629617	0.00126846	3.4015178	0.00431468
2	∞	8.21112685	-1.436799	6.774327	0.00040908	9.1531967	0.0037443
5	∞	9.84346840	-2.789102	7.054366	0.00007410	41.251854	0.0030567
7	∞	10.49963587	-3.29565	7.20398	0.00003758	72.517286	0.002725
8	∞	10.76761132	-3.4717	7.2959	0.00002851	88.50086	0.002523
9	∞	11.00741529	-3.60159	7.40582	0.00002228	102.82136	0.002290
10	∞	11.22460206	-3.91190	7.31270	0.00001782	146.1012	0.0026

of R_a , R_b and ΔR on spectroscopic and density-dependent properties are examined. Similar calculations in other central potentials is highly desirable. Particularly, it is necessary to verify the existence of such degeneracy by imposing *shell confinement* on other quantum

chemical systems. Investigation of Hellmann-Feynman theorem in the context of SCHA is desirable. Further, exploration of two-photon transition amplitude, photo-ionization cross-section, relative information in GCHA model would provide critical insight. Apart from that, it would be interesting to extend the shell confinement model to many-electron atoms.

V. ACKNOWLEDGEMENT

Financial support from BRNS, India (sanction order: 58/14/03/2019-BRNS/10255) is gratefully acknowledged. Partial financial support from SERB, India (CRG/2019/000293) is also appreciated. NM thanks CSIR, New Delhi, India, for a Senior Research Associateship (Pool No. 9033A). The authors acknowledge valuable discussion with Prof. K. D. Sen. **The authors are thankful to two anonymous referees for their constructive comments.**

Appendix A: Multipole oscillator strength and polarizability in FHA

Here, we present the *first* transition corresponding to the respective selection rule for $k = 1, 2, 3, 4$ respectively. The remaining results are provided in Supporting Material.

1. Dipole oscillator strength and polarizability

The selection rule is $\Delta\ell = \pm 1$. In s states, it changes to $\Delta\ell = 1$. However, in $\ell \neq 0$ states, $\alpha_{n\ell}^{(1)} = \alpha_{n\ell}^{(1)}(\ell - 1) + \alpha_{n\ell}^{(1)}(\ell + 1)$.

The expressions of $f_{(1s \rightarrow np)}^{(1)}(Z)$ and $f_{(2p \rightarrow ns)}^{(1)}(Z)$ are found as,

$$\begin{aligned} f_{(1s \rightarrow np)}^{(1)}(Z) &= \frac{2^8}{3Z^7} n^5 \frac{(n-1)^{(2n-4)}}{(n+1)^{(2n+4)}}, \\ f_{(2p \rightarrow ns)}^{(1)}(Z) &= \frac{2^{13}}{27Z^7} n^7 \frac{(n-2)^{(2n-5)}}{(n+2)^{(2n+5)}}, \quad (n \neq 2) \end{aligned} \tag{A1}$$

Now, using Eq. (A1) in Eq. (4), one easily gets $\alpha_{1s}^{(1)}(p)(Z), \alpha_{2p}^{(1)}(s)(Z)$ of FHA. They are obtained as,

$$\begin{aligned} \alpha_{1s}^{(1)}(p)(Z) &= \sum_{j=2}^n \frac{2^{10}}{3Z^9} j^9 \frac{(j-1)^{(2j-6)}}{(j+1)^{(2j+6)}}, \\ \alpha_{2p}^{(1)}(s)(Z) &= \sum_{\substack{j=1 \\ j \neq 2}}^n \frac{2^{19}}{27Z^9} j^{11} \frac{(j-2)^{(2j-7)}}{(j+2)^{(2j+7)}}, \end{aligned} \tag{A2}$$

2. Quadrupole oscillator strength and polarizability

In this case, the selection rule is $\Delta\ell = 0, \pm 2$. In s states it is $\Delta\ell = 2$. Similarly, in p states $\Delta = 0, 2$. Hence, $\alpha_{n\ell=1}^{(2)} = \alpha_{n\ell}^{(2)}(\ell) + \alpha_{n\ell}^{(2)}(\ell + 2)$. Moreover, for $\ell \geq 2$, $\alpha_{n\ell}^{(2)} = \alpha_{n\ell}^{(2)}(\ell - 2) + \alpha_{n\ell}^{(2)}(\ell) + \alpha_{n\ell}^{(2)}(\ell + 2)$.

The closed-form expression of $f_{(1s \rightarrow nd)}^{(2)}(Z)$, $f_{(2p \rightarrow np)}^{(2)}$ and $f_{(3d \rightarrow ns)}^{(2)}(Z)$ are obtained as,

$$\begin{aligned} f_{(1s \rightarrow nd)}^{(2)}(Z) &= \frac{2^{12}}{5Z^9} n^7 (n^2 - 4) \frac{(n-1)^{(2n-6)}}{(n+1)^{(2n+6)}}, \\ f_{(2p \rightarrow np)}^{(2)}(Z) &= \frac{2^{22}}{75Z^9} n^9 (n^2 - 1) \frac{(n-2)^{(2n-7)}}{(n+2)^{(2n+7)}}, \\ (2)_{(3d \rightarrow ns)}(Z) &= \frac{2^{17}3^7}{125Z^9} n^{13} (n^2 - 6)^2 \frac{(n-3)^{(2n-9)}}{(n+3)^{(2n+9)}}. \end{aligned} \quad (A3)$$

Now, applying Eq. (A3) in Eq. (4), one easily gets $\alpha_{1s}^{(2)}(d)(Z)$, $\alpha_{2p}^{(2)}(p)(Z)$ and $\alpha_{3d}^{(2)}(s)(Z)$ of FHA. They take the following forms,

$$\begin{aligned} \alpha_{1s}^{(2)}(d)(Z) &= \sum_{j=3}^n \frac{2^{12}}{5Z^{11}} j^{11} (j^2 - 4) \frac{(j-1)^{(2j-8)}}{(j+1)^{(2j+8)}}, \\ \alpha_{2p}^{(2)}(p)(Z) &= \sum_{j=3}^n \frac{2^{28}}{75Z^{11}} j^{13} (j^2 - 1) \frac{(j-2)^{(2j-8)}}{(j+2)^{(2j+8)}}, \\ \alpha_{3d}^{(2)}(s)(Z) &= \sum_{\substack{j=1 \\ j \neq 3}}^n \frac{2^{19}3^{11}}{5^3 Z^{11}} j^{17} (j^2 - 6)^2 \frac{(j-3)^{(2j-11)}}{(j+3)^{(2j+11)}}. \end{aligned} \quad (A4)$$

3. Octupole oscillator strength and polarizability

The selection rule is $\Delta\ell = \pm 1, \pm 3$. For $\ell = 0$, $\Delta\ell = 3$. For $\ell = 1$, $\alpha_{n\ell}^{(3)} = \alpha_{n\ell}^{(3)}(\ell + 1) + \alpha_{n\ell}^{(3)}(\ell + 3)$. Next, $\ell = 2$, the relation is, $\alpha_{n\ell}^{(3)} = \alpha_{n\ell}^{(3)}(\ell - 1) + \alpha_{n\ell}^{(3)}(\ell + 1) + \alpha_{n\ell}^{(3)}(\ell + 3)$. Further, for $\ell \geq 3$, $\alpha_{n\ell}^{(3)} = \alpha_{n\ell}^{(3)}(\ell - 1) + \alpha_{n\ell}^{(3)}(\ell - 3) + \alpha_{n\ell}^{(3)}(\ell + 1) + \alpha_{n\ell}^{(3)}(\ell + 3)$.

Now, $f_{(1s \rightarrow nf)}^{(3)}(Z)$, $f_{(2p \rightarrow nd)}^{(3)}(Z)$, $f_{(3d \rightarrow np)}^{(3)}(Z)$ and $f_{(4f \rightarrow ns)}^{(3)}(Z)$ are written as,

$$\begin{aligned} f_{(1s \rightarrow nf)}^{(3)}(Z) &= \frac{9 \cdot 2^{12}}{7Z^{11}} n^9 (n^2 - 4)(n^2 - 9) \frac{(n-1)^{(2n-8)}}{(n+1)^{(2n+8)}}, \\ f_{(2p \rightarrow nd)}^{(3)}(Z) &= \frac{2^{27}}{49Z^{11}} n^{13} (n^2 - 1)(n^2 - 16)^2 \frac{(n-2)^{(2n-10)}}{(n+2)^{(2n+10)}}, \\ f_{(3d \rightarrow np)}^{(3)}(Z) &= \frac{2^{18}3^{13}}{5^2 \cdot 7^2 \cdot Z^{11}} n^{13} (n^2 - 1)(4n^2 - 9)^2 \frac{(n-3)^{(2n-12)}}{(n+3)^{(2n+12)}}, \\ f_{(4f \rightarrow ns)}^{(3)}(Z) &= \frac{2^{34}}{245Z^{11}} n^{15} (141n^4 - 3008n^2 + 18176)^2 \frac{(n-4)^{(2n-13)}}{(n+4)^{(2n+13)}}. \end{aligned} \quad (A5)$$

Putting Eq. (A5) in Eq. (4), one easily gets $\alpha_{4f}^{(3)}(s)(Z)$, $\alpha_{1s}^{(3)}(f)(Z)$, $\alpha_{2p}^{(3)}(d)(Z)$, $\alpha_{3d}^{(3)}(p)(Z)$ and $\alpha_{4f}^{(3)}(s)(Z)$. They have following forms,

$$\begin{aligned}
\alpha_{1s}^{(3)}(f)(Z) &= \sum_{j=4}^n \frac{9 \cdot 2^{14}}{7Z^{13}} j^{13} (j^2 - 4)(j^2 - 9) \frac{(j-1)^{(2j-10)}}{(j+1)^{(2j+10)}}, \\
\alpha_{2p}^{(3)}(d)(Z) &= \sum_{j=3}^n \frac{2^{33}}{49Z^{13}} j^{17} (j^2 - 1)(j^2 - 16)^2 \frac{(j-2)^{(2j-12)}}{(j+2)^{(2j+12)}}, \\
\alpha_{3d}^{(3)}(p)(Z) &= \sum_{\substack{j=1 \\ j \neq 3}}^n \frac{2^{20} 3^{17}}{5^2 7^2 Z^{13}} j^{17} (j^2 - 1)(4j^2 - 9)^2 \frac{(j-3)^{(2j-14)}}{(j+3)^{(2j+14)}}, \\
\alpha_{4f}^{(3)}(s)(Z) &= \sum_{\substack{j=2 \\ j \neq 4}}^n \frac{2^{44}}{245 Z^{13}} j^{19} (141j^4 - 3008j^2 + 18176)^2 \frac{(j-4)^{(2j-15)}}{(j+4)^{(2j+15)}}.
\end{aligned} \tag{A6}$$

the expression of $\alpha_{n\ell}^{(4)}$ changes with alteration of ℓ values. They are,

$$\begin{aligned}
\ell = 1, \quad \alpha_{n\ell}^{(4)} &= \alpha_{n\ell}^{(4)}(\ell + 2) + \alpha_{n\ell}^{(4)}(\ell + 4), \\
\ell = 2, \quad \alpha_{n\ell}^{(4)} &= \alpha_{n\ell}^{(4)}(\ell) + \alpha_{n\ell}^{(4)}(\ell + 2) + \alpha_{n\ell}^{(4)}(\ell + 4), \\
\ell = 3, \quad \alpha_{n\ell}^{(4)} &= \alpha_{n\ell}^{(4)}(\ell - 2) + \alpha_{n\ell}^{(4)}(\ell) + \alpha_{n\ell}^{(4)}(\ell + 2) + \alpha_{n\ell}^{(4)}(\ell + 4), \\
\ell = 4, \quad \alpha_{n\ell}^{(4)} &= \alpha_{n\ell}^{(4)}(\ell - 4) + \alpha_{n\ell}^{(4)}(\ell - 2) + \alpha_{n\ell}^{(4)}(\ell) + \alpha_{n\ell}^{(4)}(\ell + 2) + \alpha_{n\ell}^{(4)}(\ell + 4).
\end{aligned} \tag{A7}$$

$f_{(1s \rightarrow ng)}^{(4)}(Z)$, $f_{(2p \rightarrow nf)}^{(4)}(Z)$, $f_{(3d \rightarrow nd)}^{(4)}(Z)$, $f_{(4f \rightarrow np)}^{(4)}(Z)$ and $f_{(5g \rightarrow ns)}^{(4)}(Z)$ as,

$$\begin{aligned}
f_{(1s \rightarrow ng)}^{(4)}(Z) &= \frac{2^{18}}{9Z^{13}} n^{11} (n^2 - 16)(n^2 - 9)(n^2 - 4) \frac{(n-1)^{(2n-10)}}{(n+1)^{(2n+10)}}, \\
f_{(2p \rightarrow nf)}^{(4)}(Z) &= \frac{2^{33}}{3^5 Z^{13}} n^{13} (n^2 - 1)(n^2 - 9)(7n^2 + 68)^2 \frac{(n-2)^{(2n-12)}}{(n+2)^{(2n+12)}}, \\
f_{(3d \rightarrow nd)}^{(4)}(Z) &= \frac{2^{20} 3^{15}}{35Z^{13}} n^{17} (n^2 - 1)(n^2 - 4)(n^2 - 21)^2 \frac{(n-3)^{(2n-13)}}{(n+3)^{(2n+13)}}, \\
f_{(4f \rightarrow np)}^{(4)}(Z) &= \frac{2^{43}}{8505Z^{13}} n^{17} (n^2 - 1)(31n^4 - 4768n^2 + 43776)^2 \frac{(n-4)^{(2n-15)}}{(n+4)^{(2n+15)}}, \\
f_{(5g \rightarrow ns)}^{(4)}(Z) &= \frac{2^{21} 5^{11}}{7 \cdot 3^6 Z^{13}} n^{19} (187n^6 - 9350n^4 + 204625n^2 + 1743750)^2 \\
&\quad \frac{(n-5)^{(2n-17)}}{(n+5)^{(2n+17)}}.
\end{aligned} \tag{A8}$$

Now, applying Eqs. (A8) in Eq. (4), one easily obtains $\alpha_{1s}^{(4)}(g)(Z)$, $\alpha_{2p}^{(4)}(f)(Z)$, $\alpha_{3d}^{(4)}(d)(Z)$,

$\alpha_{4f}^{(4)}(p)(Z)$ and $\alpha_{5g}^{(4)}(s)(Z)$. They take following forms,

$$\begin{aligned}
\alpha_{1s}^{(4)}(g)(Z) &= \sum_{i=5}^n \frac{2^{20}}{9Z^{15}} i^{15} (i^2 - 16)(i^2 - 9)(i^2 - 4) \frac{(i-1)^{(2i-12)}}{(i+1)^{(2i+12)}}, \\
\alpha_{2p}^{(4)}(f)(Z) &= \sum_{j=4}^n \frac{2^{39}}{3^5 Z^{15}} j^{17} (j^2 - 1)(j^2 - 9)(7j^2 + 68)^2 \frac{(j-2)^{(2j-14)}}{(j+2)^{(2j+14)}}, \\
\alpha_{3d}^{(4)}(d)(Z) &= \sum_{j=3}^n \frac{2^{22} 3^{19}}{35 Z^{15}} j^{21} (j^2 - 1)(j^2 - 4)(j^2 - 21)^2 \frac{(j-3)^{(2j-13)}}{(j+3)^{(2j+13)}}, \\
\alpha_{4f}^{(4)}(p)(Z) &= \sum_{\substack{j=2 \\ j \neq 4}}^n \frac{2^{53}}{8505 Z^{15}} j^{13} (31j^4 - 4768j^2 + 43776)^2 \frac{(j-4)^{(2j-13)}}{(j+4)^{(2j+13)}}, \\
\alpha_{5g}^{(4)}(s)(Z) &= \sum_{\substack{j=1 \\ j \neq 5}}^n \frac{2^{27} 5^{19}}{7 \cdot 3^6 Z^{15}} j^{23} (187j^6 - 9350j^4 + 204625j^2 - 1743750)^2 \frac{(j-5)^{(2j-19)}}{(j+5)^{(2j+19)}}.
\end{aligned} \tag{A9}$$

-
- [1] W. Grochala, R. Hoffmann, J. Feng, and N. W. Ashcroft. *Angew. Chem. Int. Ed.*, 46:3620, 2007.
- [2] E. Snider, N. Dasenbrock-Gammon, R. McBride, M. Debessai, H. Vindana, K. Vencatasamy, K. V. Lawler, A. Salammat, and R. P. Dias. *Nature*, 586:373, 2020.
- [3] K. D. Sen, J. Garza, R. Vargas, and N. Aquino. *Phys. Lett. A*, 295:299, 2002.
- [4] K. D. Sen (Ed.). *Electronic Structure of Quantum Confined Atoms and Molecules*. Springer International Publishing, Switzerland, 2014.
- [5] V. Aquilanti, H. E. Montgomery Jr., C. N. Ramachandran, and N. Sathyamurthy. *Eur. Phys. J. D*, 75:187, 2021.
- [6] J.-P. Connerade. *Eur. Phys. J. D*, 74:211, 2020.
- [7] G. Raggi, A. J. Stace, and E. Bichoutskaia. *Phys. Chem. Chem. Phys.*, 16:23869, 2014.
- [8] G. Raggi, E. Besley, and A. J. Stace. *Phil. Trans. R. Soc. A*, 374:20150319, 2016.
- [9] F. J. Dominguez-Gutierrez, P. S. Krstic, S. Irle, and R. Cabrera-Trujillo. *Carbon*, 134:189, 2018.
- [10] J. Mitroy, M. S. Safronova, and C. W. Clark. *J. Phys. B*, 43:202001, 2010.
- [11] J. Tiihonen, I. Kylänpää, and T. T. Rantala. *J. Chem. Phys.*, 147:204101, 2017.

- [12] A. Michels, J. de Boer, and A. Bijl. *Physica*, 4:981, 1937.
- [13] A. Sommerfeld and H. Welker. *Ann. Phys.*, 32:56, 1938.
- [14] T. Guillot. *Planet. Space Sci.*, 47:1183, 1999.
- [15] J. Garza, R. Vargas, and A. Vela. *Phys. Rev. E*, 58:3949, 1998.
- [16] M. Cohen C. Laughlin, B. L. Burrows. *J. Phys. B*, 35:701, 2002.
- [17] B. L. Burrows and M. Cohen. *Int. J. Quantum Chem.*, 106:478, 2006.
- [18] N. Aquino, G. Campoy, and H. E. Montgomery Jr. *Int. J. Quantum Chem.*, 107:1548, 2007.
- [19] D. Baye and K. D. Sen. *Phys. Rev. E*, 78:026701, 2008.
- [20] A. K. Roy. *Int. J. Quantum Chem.*, 115:937, 2015.
- [21] D. Puertas-Centeno, N. M. Temme, I. V. Toranzo, and J. S. Dehesa. *J. Math. Phys.*, 58:103302, 2017.
- [22] N. Sobrino-Coll, D. Puertas-Centeno, I. V. Toranzo, and J. S. Dehesa. *J. Stat. Mech.*, 8:083102, 2017.
- [23] H. E. Montgomery Jr., N. A. Aquino, and K. D. Sen. *Int. J. Quantum Chem.*, 107:798, 2007.
- [24] N. Mukherjee and A. K. Roy. *Phys. Rev. A*, 99:022123, 2019.
- [25] N. Mukherjee and A. K. Roy. *Int. J. Quant. Chem.*, 118:e25596, 2018.
- [26] N. Mukherjee, S. Majumdar, and A. K. Roy. *Chem. Phys. Lett.*, 691:449, 2018.
- [27] L. G. Jiao, L. R. Zan, Y. Z. Zhang, and Y. K. Ho. *Int. J. Quant. Chem.*, 117:e25375, 2017.
- [28] S. Majumdar, N. Mukherjee, and A. K. Roy. *Chem. Phys. Lett.*, 687:322, 2017.
- [29] N. Mukherjee and A. K. Roy. *J. Phys. B*, 53:235002, 2020.
- [30] J. R. Sabin and E. Brändas and S. A. Cruz (Eds). *The Theory of Confined Quantum Systems, Parts I and II*. Advances in Quantum Chemistry, Vols. 57 and 58, Academic Press, Cambridge, Massachusetts, 2009.
- [31] K. D. Sen (Ed.). *Statistical Complexity: Applications in Electronic Structure*. Springer International Publishing, Berlin, 2012.
- [32] L. R. Zan, L. G. Jiao, J. Ma, and Y. K. Ho. *Phys. Plasmas*, 24:122101, 2017.
- [33] S. J. C. Salazar, H. G. Laguna, B. Dahiya, V. Prasad, and R. P. Sagar. *Eur. Phys. J. D*, 75:127, 2021.
- [34] J. H. Ou and Y. K. Ho. *Int. J. Quant. Chem.*, 119:e25928, 2019.
- [35] Y. Y. He, L. G. Jiao, A. Liu, Y. Z. Zhang, and Y. K. Ho. *Eur. Phys. J. D*, 75:126, 2021.
- [36] C. Yadav, S. Lumb, and V. Prasad. *Eur. Phys. J. D*, 75:21, 2021.

- [37] L. Zhu, Y. Y. He, L. G. Jiao, Y. C. Wang, and Y. K. Ho. *Int. J. Quant. Chem.*, 120:e26245, 2020.
- [38] C. Y. Lin and Y. K. Ho. *Few. Body. Syst.*, 54:425, 2013.
- [39] K. D. Sen. *J. Chem. Phys.*, 122:194324, 2005.
- [40] M. Cohen B. L. Burrows. *Mol. Phys.*, 106:267, 2008.
- [41] K. D. Sen and P. C. Schmidt. *Phys. Rev. A*, 23:1026, 1981.
- [42] J. G. Kirkwood. *Phys. Z*, 33:57, 1932.
- [43] R. A. Buckingham. *Proc. R. Soc. London, Ser. A*, 160:94, 1937.
- [44] R. M. Sternheimer. *Phys. Rev.*, 96:951, 1954.
- [45] V. I. Pupyshev and H. E. Montgomery Jr. *Int. J. Quant. Chem.*, 119:e25887, 2019.
- [46] E. M. Nascimento, F. V. Prudente, M. N. Guimar aes, and A. M. Maniero. *J. Phys. B*, 44:015003, 2011.
- [47] A. L. Efros and D. J. Nesbitt. *Nature Nanotechnology*, 11:661, 2016.
- [48] Z. Fei, Z. Wang, D. Li, F. Xue, C. Cheng, Q. Liu, X. Chen, M. Cui, and X. Qiao. *Nanoscale*, 13:10765, 2021.
- [49] H. Peng, C. Rao, N. Zhang, X. Wang, W. Liu, W. Mao, L. Han, P. Zhang, and S. Dai. *Angew. Chem. Int. Ed.*, 57:8953, 2018.
- [50] C. Rao, C. Peng, H. Peng, L. Zhang, W. Liu, X. Wang, N. Zhang, and P. Wu. *ACS Appl. Mater. Interfaces*, 10:9220, 2018.
- [51] T. Raj kumar, G. Gnana kumar, and Arumugam Manthiram. *Adv. Energy Mater.*, 9:1803238, 2019.
- [52] Y. Lai, W. Xia, J. Li, J. Pan, C. Jiang, Z. Cai, C. Wu, X. Huang, T. Wang, and J. He. *Electrochimica Acta*, 375:137966, 2021.
- [53] M. Fan, D. Liao, M. F. Aly Aboud, I. Shakir, and Y. Xu. *Angew. Chem. Int. Ed.*, 59:8247, 2020.
- [54] A.-C. Shi and B. Li. *Soft Matter*, 9:1398, 2013.
- [55] M. R. Khadilkar and A. Nikoubashman. *Soft Matter*, 14:6903, 2018.
- [56] L. Qin, C. Li, X. Li, X. Zhang, C. Shen, Q. Meng, L. Shen, Y. Lu, and G. Zhang. *J. Mater. Chem. A*, 8:1929, 2020.
- [57] M. Zhang, C. Xiao, X. Yan, S. Chen, C. Wang, R. Luo, J. Qi, X. Sun, L. Wang, and J. Li. *Environ. Sci. Technol.*, 54:10289, 2020.

- [58] D. E. Hastings and H. D. H. Stöver. *ACS Appl. Polym. Mater.*, 1:2055, 2019.
- [59] G. Gnana kumar, S.-H. Chung, T. Raj kumar, and Arumugam Manthiram. *ACS Appl. Mater. Interfaces*, 10:20627, 2018.
- [60] W. Shuang, H. Huang, L. Kong, M. Zhong, A. Li, D. Wang, Y. Xu, and X.-H. Bu. *Nano Energy*, 62:154, 2019.
- [61] J. Wang, L. Zhu, F. Li, T. Yao, T. Liu, Y. Cheng, Z. Yin, and H. Wang. *Small*, 16:2002487, 2020.
- [62] A. K. Roy. *Mod. Phys. Lett. A*, 29:1450104, 2014.
- [63] A. K. Roy. *J. Math. Chem.*, 52:1405, 2014.
- [64] A. K. Roy. *Mod. Phys. Lett. A*, 29:1450042, 2014.
- [65] S. Majumdar and A. K. Roy. *Quant. Rep.*, 2:189, 2020.
- [66] S. Majumdar and A. K. Roy. *Int. J. Quant. Chem.*, 121:e26630, 2021.
- [67] M. Das. *Phys. Plasmas*, 19:092707, 2012.
- [68] A. Dalgarno. *Adv. Phys.*, 11:281, 1962.
- [69] L. Zhu, Y. Y. He, L. G. Jiao, Y. C. Wang, and Y. K. Ho. *Phys. Plasmas*, 27:072101, 2020.
- [70] I. Bialynicki-Birula and J. Mycielski. *Commun. Math. Phys.*, 44:129, 1975.
- [71] J. S. Shiner, M. Davison, and P. T. Landsberg. *Phys. Rev. E*, 59:1459, 1999.
- [72] A. Solyu. *Phys. Plasmas*, 19:072701, 2012.
- [73] L. G. Jiao, Y. Y. He, Y. Z. Zhang, and Y. K. Ho. *J. Phys. B*, 2021.
- [74] S. Paul and Y. K. Ho. *Phys. Rev. A*, 79:032714, 2009.
- [75] M. K. Bahar and A. Solyu. *Phys. Plasmas*, 092703:21, 2014.
- [76] M. K. Bahar, A. Soyulu, and A. Poszwa. *IEEE Trans. Plasma Sci.*, 44:2297, 2016.
- [77] Y.-D. Jung. *Phys. Plasmas*, 332:2, 1995.
- [78] Y.-D. Jung and J.-S. Yoon. *J. Phys. B*, 29:3549, 1996.
- [79] M. Y. Song and Y.-D. Jung. *Phys. Plasmas*, 36:2119, 2003.
- [80] C. Y. Lin and Y. K. Ho. *Eur. Phys. J. D*, 57:21, 2010.
- [81] C. Y. Lin and Y. K. Ho. *Comp. Phys. Commun.*, 182:125, 2011.
- [82] D. Baye. *Phys. Rev. A*, 86:06254, 2012.
- [83] K. F. Herzfeld. *Phys. Rev.*, 29:701, 1927.